Manufacturing and characterization of blended PVDF/PVDF-TrFE polymers: a study towards future sensor applications

by

Zongyu Wang

A thesis submitted in partial fulfillment of the requirements for the degree of

Master of Science

Department of Mechanical Engineering
University of Alberta

Abstract

Poly (vinylidene fluoride) (PVDF) and its copolymers received increasing attention due to their electroactive properties and lower processing cost in comparison to the conventional piezoelectric ceramic materials, which are widely used in electronics, energy harvesting, biochemistry, and sensor areas. PVDF-Trifluoroethylene (PVDF-TrFE) is a copolymer of PVDF, and this copolymer presents superior piezoelectric response and good ferroelectric properties, but has considerably higher cost compared to PVDF. For many applications, it is desirable to find a blend of PVDF and PVDF-TrFE that presents an optimal combination of good properties and reasonable cost. This can be done by investigating the effects of using different weight ratios of PVDF/PVDF-TrFE and different thermal and electrical treatments on the mechanical and piezoelectric properties of the blended PVDF/PVDF-TrFE samples.

Consequently, this study reports on manufacturing and characterization of blended PVDF/PVDF-TrFE using extrusion and spin-coating. Prepared specimens are analyzed without any further treatment and with post-manufacturing treatments (annealing, poling, poling heating, annealing poling, annealing poling heating) to study the effect of treatments on the properties. The weight ratio of PVDF-TrFE was set at 0, 10, 20, 30 and 100 wt.% to test the mechanical properties of the extruded PVDF/PVDF-TrFE filaments. As the electrical poling was not applicable for the long filament due to safety concerns, only annealing treatment was applied in the mechanical test. As the PVDF-TrFE content increased, the corresponding elastic modulus and ultimate tensile strength decreased, and the decline in elastic modulus followed the rule of mixtures. The annealing treatment was found to impose a negative effect on the elastic modulus and ultimate tensile strength, which might result from spherulite formation during this thermal treatment. An in-house built pendulum impact test set-up was created to investigate the

piezoelectric response of the blended PVDF/PVDF-TrFE polymer using spin-coated samples. The relationship between the electroactive semi-crystalized β-phase content and the output voltage was carried out studied by FT-IR characterization. The PVDF/PVDF-TrFE ratio of 70/30 and 80/20 rendered the highest and lowest averaged β-phase content, at 33.81% and 29.55 respectively, while the percentage for pure PVDF and PVDF-TrFE was 32.16% and 39.90% respectively. The enhancement of β-phase under treatments was found to be more effective in the pure PVDF and PVDF-TrFE, especially under the annealing and annealing poling heating. After blending with 10 to 30wt.% of PVDF-TrFE, PVDF generally witnessed a rise in the magnitude of the maximum output voltage during pendulum impact test. For a single sample, the highest magnitude of output voltage (1.76 V) was shown in one 90/10 sample under annealing poling, which was even higher than the maximum value (1.43 V) for pure PVDF-TrFE. The lowest electrical output level was found in 80/20, which was consistent with its low β-phase content. A sensitivity analysis identified that the pure PVDF-TrFE samples had the highest magnitude of sensitivity, which was attributed to the superior energy conversion efficiency of this material. 90/10 and pure PVDF samples presented better sensitivity than 70/30 and 80/20. The low chain mobility and presence of interfaces in 70/30 and 80/20 might have decreased the energy conversion.

Overall, this study demonstrates the feasibility of blending PVDF and electroactive PVDF-TrFE as an enhancement towards electrical response to mechanical impact under specific thermal and electrical treatments. Blended PVDF/PVDF-TrFE provides a cost-saving possibility for the piezoelectric polymer applications.

Preface

This research was conducted under the co-supervision of Dr. Cagri Ayranci and Dr. Tian Tang from Department of Mechanical Engineering at University of Alberta. The experiment of FT-IR characterization, spin coating, and pendulum impact tests in Chapter 2 was done with assistance from Ms. Jiawei Chen [1]; however, the analysis and writing and discussion of the findings were done entirely by me. The literature review in Chapter 1, extrusion and mechanical test in Chapter 2, and all data analysis in Chapter 3 were my original work.

A version of Chapter 3 of will be prepared for submission to a journal after the submission of this thesis.

_____

[1]Jiawei Chen is a PhD student in Dr. Cagri Ayranci and Dr. Tian Tang's research groups.

Acknowledgement

I would like to express my sincerest appreciation to my supervisors, Dr. Cagri Ayranci and Dr. Tian Tang, for their consistent support during the past two years. Their patient guidance and encouragement provided me the greatest energy in my research and thesis writing. Dr. Ayranci is patient and inspirational, always helping improve my work with his expertise, generousness, and great sense of humor. Dr. Tang is warm-hearted, professional and decisive, always offering me the valuable suggestions at the key moment with fulfilled passion. I also would like to thank Dr. Mark McDermott for granting the access to his lab and usage of spin coater.

It is my honor and luck to meet and work with not only my supervisors but also our research fellows: Mr. Eyup Demir, Dr. Irina Garces, Ms. Jiawei Chen, and Mr. Yu Chen, without them I cannot complete my research during this pandemic.

Finally, I would express my gratitude to my parents and family members who always understand and stand behind me, and I can feel their love and support even though across the Pacific Ocean. My mom is such a wonderful and strong woman, and she is my role model and life mentor. My dad teaches me the to see this world in diverse perspectives and he will always be hero.

Table of Contents

List of Tables

List of Figures

List of Symbols

(+) = Positive Peak Only Mode

(+;-) = Positive Peak and Negative Peak Mode

(-) = Negative Peak Only Mode

(-;+) = Negative Peak and Positive Peak Mode

A = Absorbance

A_o = Original cross section area

AC = Alternating Current

AFM = Atomic Force Microscopy

CNT = Carbon Nanotube

CSA = Cross Section Area

D = Diameter of Steel Ball

DC = Direct Current

DMF = Dimethylformamide

DSC = Differential Scanning Calorimetry

DSMO = Dimethyl sulfoxide

ES = Electrospinning

Ec = Critical Energy

F = Load in Tensile Test

$F( )$ = Fraction of a Type of Phase

FDM = Fused Deposition Modelling

FE = Ferroelectric

FT-IR = Fourier Transform Infrared

F_{ave} = Average force

FeFET = Ferroelectric Field Effect Transistor

H = Peak Height/Peak valley difference/Peak area

IAR = Integrated Area Ratio

ITO = Indium Tin Oxide

K = Absorbance Coefficients

L = Length of Impact sensor

M = Mass of Steel Ball

MEK = Methyl Ethyl Ketone

MES = Melt Electrospinning

MFI = Melt Flow Index

Mw = Molecular Weight

OVDF = Vinylidene Fluoride Oligomers

PAR = Peak Area Ratio

pk-pk = Peak-to-Peak

PE = Paraelectric

PHDR = Peak height Difference Ratio

PHR = Peak Height Ratio

PID = Proportional Integral Derivative

POM = Polarized Optical Microscope

Pr = Remnant Polarization

PVD = Physical Vapor Deposition

PVDF = Poly (vinylidene fluoride)

PVDF-CTFE = Poly(vinylidene fluoride-co-chlorotrifluoroethylene)

PVDF-HFP = Poly(vinylidene fluoride-co-hexafluoropropylene

PVDF-TrFE = Poly(vinylidene fluoride-co-trifluoroethylene)

PWM = Pulse Width Modulation

R = Ratio for FT-IR Spectroscopy Analysis

Rpm = Rotation per minute

SEA = Solvent Evaporation Assisted

SEM = Scanning Electron Microscope

SSR = Solid State Relay

Se = Sensitivity

Tc = Curie Temperature

Tm = Melting Temperature

v = Velocity of Steel Ball

V = Output voltage

WAXD = Wide Angle X-ray Diffraction XRD = X-Ray Diffraction

ZnO = Zinc Oxide

d = Piezoelectric Coefficient

k = Electromechanical Coupling Factor

l = Effective gauge Length of Filament

Δl = Displacement

σ = Nominal Stress

ε = Strain

Subscript 1 = Initial

Subscript 2 = Rebounded

Subscript 31 = Response along Transverse Direction

Subscript 33 = Response along Longitudinal Direction

Subscript α = Trans-gauche Conformation Phase

Subscript β = All-trans Planar Form Phase

Subscript γ = Zigzag Form Phase

Chapter 1. Literature review

1.1. PVDF

PVDF is a semi-crystalline polymer consisting of α-, β- and γ- phases representing trans-gauche conformation, all-trans planar and zigzag form, respectively [1]. As shown in Figure 1.1, for the β-phase structure, all the substituted fluorine and hydrogen atoms are at the opposite side of the molecular chain; therefore, they generate a net dipole moment and the polymer chain to go through twisting and tilting. The mutual repulsion within fluorine atoms causes instability in the all-trans structure (β-phase). Due to the instability, a phase transition exists from all-trans molecules to trans-gauche (α-phase) above the curie temperature (T_c), where sufficient thermal energy would be generated to induce the segmental rotation [2]. According to Martins et al., β and γ phases are both electrically active, while β-phase renders the highest dipole moment per unit cell [3]. Thus, within the three major crystalline structures, it is the β-phase that contributes to the remarkable ferroelectric, piezoelectricity and electromechanical properties of PVDF [2]. Specifically, ferroelectricity indicates that the direction of spontaneous electric polarization of ferroelectric material could be reversed under an external electric field. Piezoelectricity means that an electrical potential could be induced when applying mechanical stress or strain on a dielectric material. Electromechanical properties describe the efficiency between electrical and mechanical behaviors. For piezoelectric materials, the linear relationship between generated electrical potential and the applied stress/strain is advantageous for applications like strain gauge sensors or actuators [4]. PVDF also provides decent biocompatibility, thermal stability, and chemical resistance, offering a wide range of prospect in biological and medical applications. Moreover, PVDF has high mechanical strength, easy processability and relatively affordable cost (600 USD/500g) compared to polymers with similar properties; therefore, this material is attractive for various industrial purposes [5].
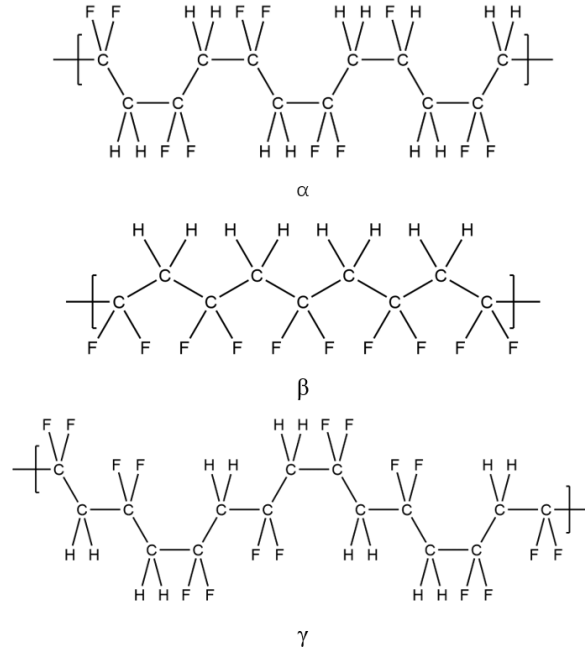
Figure 1.1. Polymer chain conformation of α-, β- and γ- phase. (Adopted from Martins et al. [3])

However, the crystallinity and β-phase in PVDF are low unless the material is subjected to treatments, such as electrical poling, thermal annealing, and mechanical stretch to improve the crystalline orientation [2]. Treatments like electric poling and thermal annealing are capable of improving the crystallinity and therefore increase β-phase content of this material.

1.2. Electrical poling

Electrical poling is an effective way to improve the aforementioned favorable properties. Under high electric field and elevated temperature, poling is capable of promoting the reorientation of molecular dipoles inside the crystallites along the electric field direction, thus improving the crystallinity and piezoelectricity properties [6].

As shown in Figure 1.2, there are several types of poling processes, such as (a) in-situ poling [7] [8], (b) Corona poling [9], (c) Contact poling, or a combination of them [10]. Specifically, the in-situ poling is popular in additive manufacturing processes such as Fused Deposition Modelling (FDM) [7] and solvent evaporation-assisted (SEA) 3D printing [8] [11].
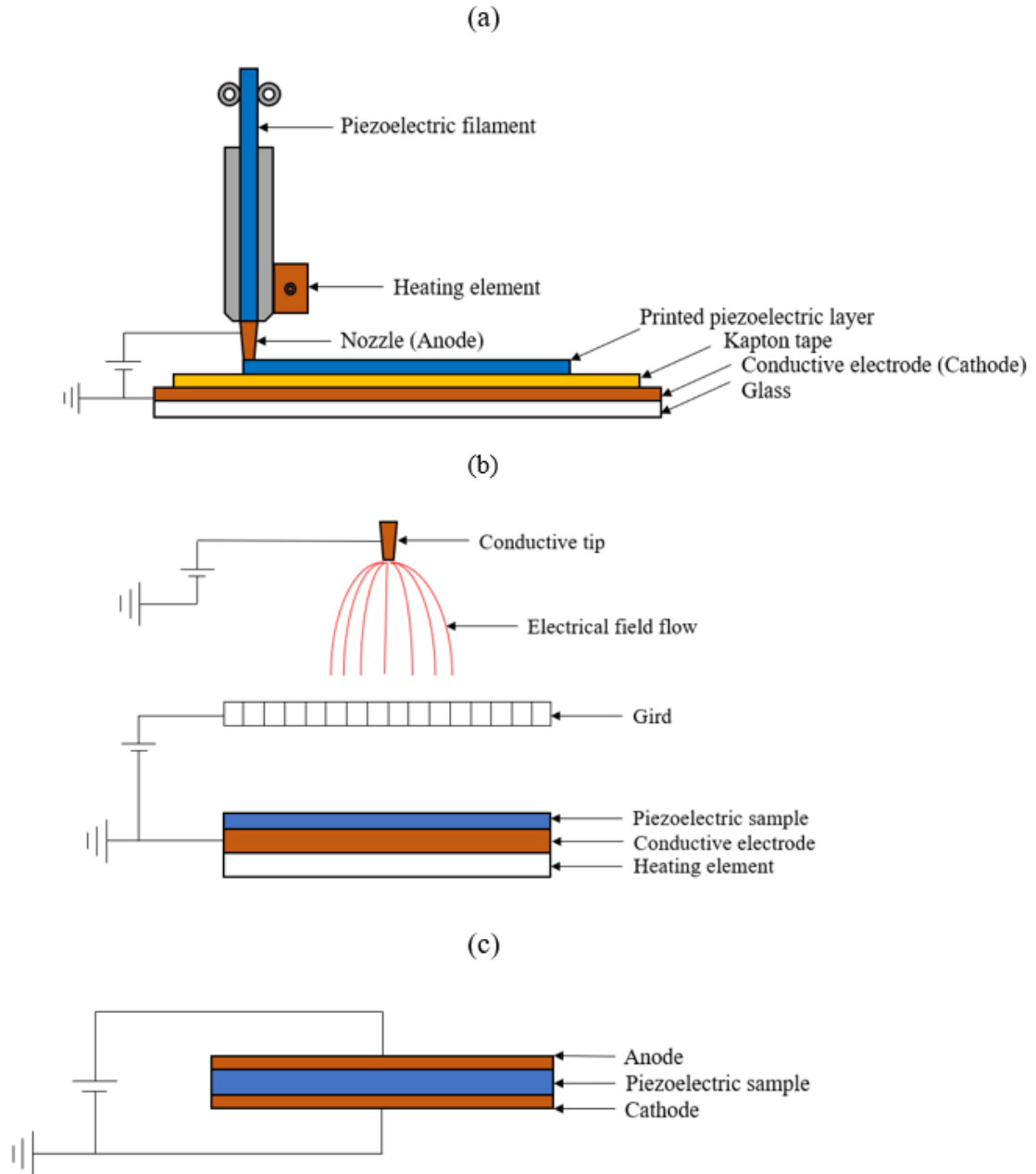
Figure 1.2. Schematic view of electrical poling setup including (a) In-situ poling (b) Corona poling (c) Contact poling.

For the setup of in-situ poling, shown in Figure 1.2 (a), the positive terminal of the power supply is connected to the conductive nozzle, while the negative terminal is connected to the conductive layer at the printing bed. The major advantage of in-situ poling is that the material manufacturing and poling can be operated simultaneously. Therefore, the material can be poled

during the molten state where the electrically inductive components are easier to be aligned and oriented. Also, the time consumed for poling can be dramatically minimized. However, the drawback of this process is that the electrical components on the connected machine might be damaged due to the high voltage.

In comparison, corona poling set up could be more complex. The setup shown in Figure 1.2 (b) requires a high voltage (~10-20 kV) between the air above the sample and ground to overcome the resistance within the non-contact distance and reach an effective electric field. Additionally, there is usually an extra conductive grid between the positive terminal and the sample to make the electrical field more uniform, where a lower grid voltage (~1-2 kV) is applied between the grid and the ground [9]. Sometimes for set-up simplification, the grid setup might be omitted [12].

In some applications, due to the large contact area of membranes and thin films, a contact poling shown in Figure 1.2 (c) is more favorable, where the anode and cathode of the power supply can adhere to poled materials. Depending on the sample thickness and the breakdown voltage of the material, the magnitude of contact poling voltage ranges from hundreds to a few thousand of volts to maintain the electric field strength between 1 to 100MV/m [8] [10].

Nonetheless, these electrical poling processes may increase operational cost and time on the fabrication. Additionally, the introduction of conductive micro or nano fillers could further improve the electroactivity of PVDF and β-phase content, including metal oxide like ZnO nanoparticle [13] or carbon-based additive such as carbon nanotube (CNT) [14] and graphene [15] [16]. However, the usage of specific additives might drastically increase the costs and bring environmental concerns; thus, this was not considered in our research.

1.3. Annealing

Thermal annealing is a crucial process for piezoelectric polymers, where at specific temperatures the material structure and some of the mechanical properties might be altered [17]. As the curie temperature of PVDF (T_c) (~195 °C) is higher than its melting point (T_m) (~170 °C), annealing at specified temperatures (below T_m) for different time periods could alter the crystalline phase that exists in PVDF [1]. According to Kaur et al., their solution-casted PVDF/DMF samples were annealed at different temperatures for 5 hrs accordingly, and the polar β-phase was found to coexist with α-phase up to annealing temperature of 100 °C. However, this

coexistence was fully transformed to α-phase when the annealing temperature exceeded 100 °C [18]. Also, according to Satapathy et al., who investigated the effect of annealing on the conversion between β- and γ- phases by using a polar solvent DMSO in solution casting, the maximum β- phase content was observed in the PVDF films when the samples were annealed at 90 °C for 5 hrs [19].

According to Buchdahl et al., annealing process may improve the crystallinity and crystalline orientation, thus enhancing the modulus and yield strength, but at the cost of weakening the elongation to yield and to break [20]. On the other hand, it was usually noted that a more obvious spherulitic (larger size) formation could be induced by either annealing or slow cooling process, with the increase in degree of crystallinity [21]. The spherulites tend to break along their radii when they grow to a large size. Also, fractures often occur along the boundaries between defected spherulites. As a result, microscopically, annealing under the melting point or cooling from over the melting point could lead to the growth of spherulite size and lamella thickness. In a macroscopic view, the influence above might bring brittleness.

Li et al. investigated the effect of annealing time (0, 0.5, 1, and 4 hours) and temperature (140, 150, and 160° C) on the mechanical properties of melt spun hollow PVDF fiber. The elongation at break seemed not to present a clear correlation with the annealing time or temperature, as these annealing parameters might influence crystallinity and orientation separately. The elastic modulus of PVDF fibers increased after annealing for less than 1 hour, while experiencing a decline under annealing for a longer period. 140° C was found to be an optimal annealing temperature, which could improve both elastic modulus and ultimate tensile strength, and this enhancement can be attributed to increased crystallinity and comparative change of orientation at this temperature, which was confirmed by their differential scanning calorimetry (DSC) and wide-angle X-ray diffraction (WAXD) results [22].

According to Martins et al., when selecting piezoelectric materials for sensor applications, the main piezoelectric coefficients (d_{33} and d_{31}), electromechanical coupling factor (k_{33}), and dielectric constant (ε') should be considered [3]. For the main piezoelectric coefficients, the second subscript denotes the direction of stress applied and the first subscript denotes the direction of piezoelectric response. As shown in Figure 1.3, d_{33} is defined as the longitudinal coefficient, representing the electrical output is along the direction of stress applied (compressive). Therefore, d_{33} is widely used to evaluate pressure sensor. d_{31} refers to the

transverse piezoelectric coefficient, representing the electrical output is perpendicular to the direction of stress applied (tensile) [5]. In order to quantify relationship between the applied stress/strain and the electrical reaction along the stress/strain direction, the d_{33} was frequently mentioned in energy harvesting research and this number could be measured by a specialized d_{33} meter. Additionally, k_{33} represents the conversion efficiency between electrical and mechanical energy.
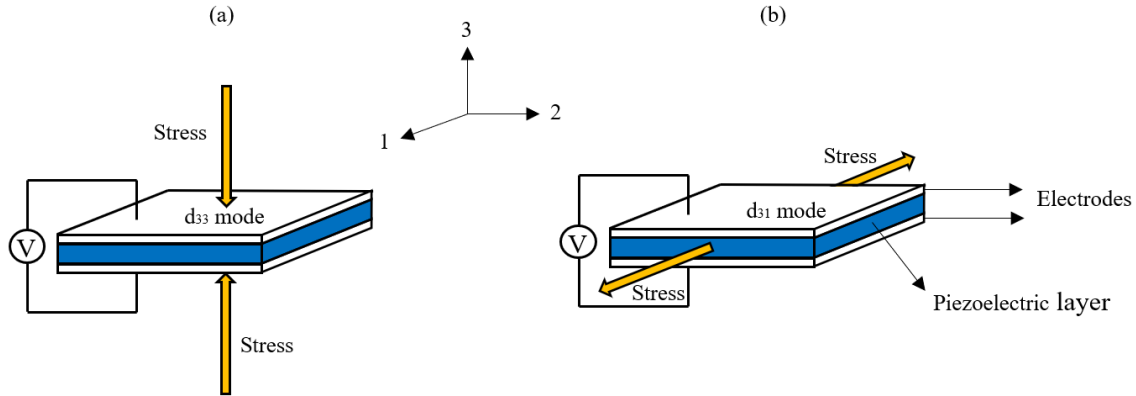
Figure 1.3. The direction of stresses applied and corresponding piezoelectric response for (a) d_{33} and (b) d_{31}.

1.4. Copolymers of PVDF

For PVDF, due to its low crystallinity and electroactive β-phase content, the corresponding piezoelectric behavior (d_{33}) and electromechanical conversion efficiency (k_{33}) remains at a relatively low level. By introducing specific functional groups into PVDF, some copolymers of PVDF were synthesized, in order to explore the enhancement of the relevant properties. The three major PVDF-based copolymers in sensor applications are compared as follows.

1.4.1. PVDF-Hexafluoropropylene (PVDF-HFP)

According to Martins et al., after introducing amorphous HFP into PVDF (Figure 1.4), PVDF-HFP could be widely used as the electrolytes of rechargeable lithium batteries due to its chemically inert nature. PVDF-HFP presents low β-phase and crystallinity level [3]. Therefore, this material requires specific treatment to improve its crystallinity and corresponding ferroelectricity and piezoelectricity. For example, rapid cool-down quenching procedure is usually applied. After quenching, its d_{33} can reach -24 pC/N [23], which is slightly higher than PVDF (-22 pC/N) but still much lower in comparison to PVDF-CTFE and PVDF-TrFE (-38

6

pC/N) without any treatment [24]. Besides, its piezoelectric properties cannot be maintained for a long period after the treatment. It was also said that the bulkier HFP units in the PVDF chains was regarded as defect and an unstable factor for electroactive β-phase [25]. In summary, this copolymer of PVDF was not chosen for the application in this thesis work.
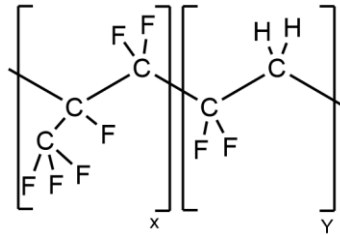
Figure 1.4. Schematic of the repeating units in PVDF-HFP (adopted from Martins et al. [3]).

1.4.2. PVDF-Chloride trifluoride ethylene (PVDF-CTFE)

PVDF can also be modified with CTFE (Figure 1.5) in the molecular chain. Although PVDF-CTFE provides high d_{33} value, its loose structure with bulky molecular weight increases the instability of its piezoelectric properties. Besides, in sensor applications, after applying stress/strain to the material, the so-called electro-strictive response from PVDF-CTFE is non-linear and irreversible, which dramatically increases the difficulties of predicting the piezoelectric behaviors and decreases the repetition of usage. In comparison, the piezoelectric behaviors in PVDF and PVDF-TrFE are linear and reversible. Therefore, PVDF-CTFE was not selected as the sensor material in this research.
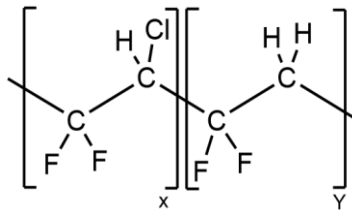
Figure 1.5. Schematic of the repeating units in PVDF-CTFE (adopted from Martins et al. [3]).

1.4.3. PVDF-Trifluoroethylene (PVDF-TrFE)

PVDF-TrFE (Figure 1.6) is one of the most investigated copolymers of PVDF. The Trifluoroethylene monomer in the PVDF polymer chain presents strong steric hindrance from the added fluorine atoms. Therefore, PVDF-TrFE becomes a copolymer that has steady β-phase content after solidification without further poling or mechanical stretching [16]. However, only if the TrFE composition in PVDF-TrFE is between 20 mol% and 50 mol%, this copolymer has a

7

great crystallinity and spontaneously formed highly crystalized β-phase. Therefore, PVDF-TrFE also showed superior electrically active properties [3]. Although PVDF-TrFE has the most favorable performances, due to the difficulties of storage and transport for its toxic Trifluoroethylene monomer, the price of PVDF-TrFE is prohibitively high for many commercial applications [7], approximately $3,300 USD/500g, which is 10 times the cost of PVDF.
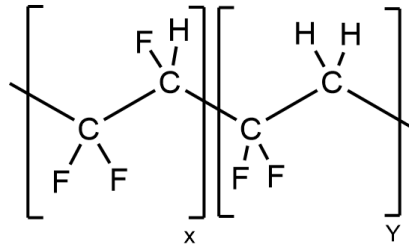
Figure 1.6. Schematic of the repeating units in PVDF-TrFE (adopted from Martins et al. [3]).

Furthermore, by introducing a comonomer into PVDF-TrFE, the terpolymers like PVDF-TrFE-CTFE could be synthesized. This could lead to transition of properties from ferroelectric to relaxor ferroelectric. As a result of the expanded interchain distance between the polymer chains, there are more space for the alignment of dipoles, and the α-phase could be converted to β and γ. Therefore, the relaxor ferroelectric material not only provides a higher electro-strictive strain response but also acquires better dielectric properties in comparison to the regular ferroelectric polymers [16]. However, the synthesis of this type of material is more complicate and expensive.

Different from PVDF, the PVDF-TrFE copolymer exhibits a T_c under the T_m, enabling people to investigate its transition from ferroelectric (FE) to paraelectric (PE) phases [1]. Besides poling and stretching, an annealing process at a temperature between the first Curie point (slightly above 100-120 ℃) and melting point (under 130-150℃) is usually applied to improve the crystallinity of PVDF-TrFE. According to Mohamad et al. [26], this crystallinity enhancement could be ascribed to the fact that the structure of C-F molecules in PVDF-TrFE was aligned in polarized conformation, thus improving its dipole orientation. Another explanation was that the increased chain mobility of PVDF-TrFE might lead to the growth in the lamella thickness [27]. Consequently, the annealed PVDF-TrFE samples were reported to reach 80-90% crystallinity, whereas PVDF samples only level off at 50% after annealing.

Mohamad et al. also carried out systematic tests using different annealing temperatures on spin-coated PVDF-TrFE thin film with thickness of around 250 nm. By subjecting each sample to

2 hours of annealing process, it was found that as the annealing temperature increased from 100° C to 160° C, the crystallite sizes grew gradually, and therefore the crystallinity of PVDF-TrFE thin films were elevated by the development of crystallite length. However, while the sample annealed at 160° C had the highest crystallinity, its remnant polarization (P_r) remained at a lower level in comparison to others, which was due to the fibrous-like 'separation' and defects like leakage current as well as parasitic capacitance [26]. Overall, the morphology of the PVDF-TrFE spin-coated samples generated better polarization when annealing temperature was at 120 ° C as these thin films rendered more closely elongated crystallites than other annealed samples. Meng et al. applied annealing on extruded pure PVDF-TrFE thin films at 140° C for 24 hours to enhance the corresponding electroactive properties [28]. Thereafter, the same group, Meng et al. took 2 hours for annealing on the blended PVDF/PVDF-TrFE thin film at the optimized 120° C, indicating the decline of optimized annealing temperature and time after blending PVDF with PVDF-TrFE [27].

In summary, thermal annealing process could be beneficial to the mechanical and electrical properties of both PVDF and PVDF-TrFE; however, the maloperation of annealing temperature might impose negative effect on these properties.

1.5. Blending PVDF and PVDF-TrFE

PVDF provides better mechanical properties and reasonable price, which attracts market's attention. On the other hand, PVDF-TrFE exhibits favorable electrical performances but has high cost; therefore, the need between these two perspectives should be balanced. To reduce the material cost while maintaining the favorable properties of PVDF-TrFE, some researchers proposed to mix PVDF and PVDF-TrFE.

Theoretically, polymer blends were categorized into two types according to Paul et al. [29]. Firstly, miscible or homogeneous polymer blend represented that the mixed polymers presented a single-phase structure, where only one glass transition temperature was discovered. Secondly, immiscible or heterogeneous polymer blends meant the existence of different phases, where separate glass transition temperatures could be observed. Nevertheless, if specific compatibility and optimized properties are observed after blending the polymers, this polymer blend could be considered compatible. After the combination, compatible polymer blends are expected to exhibit uniform physical properties at a macroscopic scale by ensuring adequately strong interaction

among the components in the polymer blends. Disadvantageous features due to the defects like phase separation [30] should be avoided. In two-phase or multi-phase polymer blends, the adhesion between phases could affect most properties and applications, especially mechanical properties [31].

1.5.1. Miscibility of PVDF and PVDF-TrFE

First of all, it is important to understand the miscibility and existence of phases between PVDF and PVDF-TrFE when blending them into further applications. Tracing back to 1990, Tanaka et al. firstly verified the immiscibility of the PVDF/PVDF-TrFE blends by observing two distinct transition temperature peaks in the DSC test for the solution mixed polymers with different blended weight ratios [32]. Thereafter Pinheiro et al. also showed immiscible crystalline phases in the polymer blends according to the SEM results, while they also found out that the appearance of PVDF-TrFE caused the asymmetric distribution of the ringed spherulite in the PVDF-based interlamellar region [33]. Therefore, it was very likely that the two polymers are at least partially miscible in the liquid form and possibly in the amorphous solid state. Although the correlation between microscopic morphology and macroscopic properties of this blended polymer was not compared at the early stage, the research on miscibility was a good start for further investigation on interaction between these PVDF and PVDF-TrFE.

1.5.2. Spin coating of OVDF/PVDF-TrFE

The oligomer of vinylidene fluoride (OVDF) is the short-chain VDF molecule, enabling the polymer to form an ordered structure. The blending the OVDF and PVDF-TrFE was investigated by Zhang et al., where the spin-coating method was used for preparing samples. The thin films with nano-scale thickness were expected to provide decent ferroelectric properties. They utilized XRD and FTIR to find out the variations of α-, β- and γ- phase fractions corresponding to different OVDF/PVDF-TrFE ratios. A significant drop in the β-phase content was observed when the ratio of OVDF/PVDF-TrFE exceeds 60%. Also, their DSC test results along with hysteresis loop measurement confirmed that the ferroelectricity of the blended polymer remained at a high level when the OVDF ratios ranged from 0% to 40%, while a drastic decay occurred after 60%. As a result, the pure PVDF-TrFE showed superior ferroelectric properties in all weight ratios [34]. Nonetheless, this research only discussed ferroelectric aspects, instead of further piezoelectric application. Besides, OVDF gradually faded out of the market duo to its unstable performance, high cost and limited application.

1.5.3. Solution casting

Jia et al. used solution casting to prepare the blended PVDF/PVDF-TrFE thin films to investigate the effect of PVDF-TrFE weight ratios on morphology, thermal and electroactive properties. As the PVDF-TrFE content increased, a decreasing trend was found in the lamella thickness and enthalpy of this polymer. This trend indicated that the high steric hindrance from fluoride atom can inhibit the crystallization, thus considerable amount of β-phase nucleated in PVDF. When the PVDF-TrFE reached 50wt.%, the solution-casted sample showed the highest d33 value. Unlike pure PVDF, some defects like porous structures were found on the samples after blending with PVDF-TrFE. This defect was corresponding to the disappearance of spherulite-dominant morphology, possibly resulting from the higher energy required to move TrFE molecular chains during the crystallization process. After the evaporation of the solvent, the porous structure occurred on the flat surface, which might affect the measured properties and interfere with the results [35]. Therefore, improvements on manufacturing methods and parameters could be attempted to avoid this problem.

1.5.4. Sol-gel

Park et al. examined the application of blending PVDF/PVDF-TrFE with the sol-gel method for Organic Field-Effect Transistors (OFET). Only the samples with 50 and 70wt.% PVDF-TrFE content was fabricated and compared to the PVDF and PVDF-TrFE OFET. For this application, as the PVDF-TrFE weight ratio reached 70wt.%, and the PVDF/PVDF-TrFE sample was found to show even higher ferroelectric and electrical characteristics of the OFET than the ones in pure PVDF-TrFE [36]. However, a small number of samples might not comprehensively explain the effect of PVDF-TrFE weight ratios on the ferroelectric properties of PVDF/PVDF-TrFE OFET. Large amount of PVDF-TrFE usage in this application might dramatically increase the material cost.

1.5.5. Electrospinning

Kibria et al. attempted to fabricate electrospinning based PVDF-TrFE nanofiber for acoustic sensor applications. Three grades of PVDF-TrFE were used with PVDF/TrFE ratios of 60:40, 70:30 and 80:20, and the solution was prepared based on MEK solvent. PVDF was used to dilute PVDF-TrFE solution, since it could optimize the fiber surface smoothness and improve the fiber porosity. FT-IR and XRD characterizations were performed although they were not used to calculate the β-phase content or d33 results. According to the SEM results, the porosity of the

electrospun PVDF-TrFE fibers varied with different PVDF/TrFE ratios. As specific PVDF dilution was applied, the pore sizes of the group of 60:40 pores can be dramatically minimized. In comparison, larger pore sizes were still observed in the samples of 70:30 and 80:20 after PVDF dilution [37]. Nevertheless, the authors did not mention detailed data for their dilution process and the effect of PVDF dilution percentage on the electroactive properties of PVDF-TrFE was not analyzed in this paper.

1.5.6. Extrusion (Melt-mixing)

Apart from those solution-mixed methods, Meng et al. carried out systematic research about the effect of PVDF-TrFE weight ratios on the ferroelectric properties of blending PVDF/PVDF-TrFE by using the extrusion method. The weight ratios of PVDF-TrFE thin film were specified from 10 to 40 wt. % in a step of 10wt.%, where the pure PVDF and PVDF-TrFE were also investigated. The DSC tests involved three steps including first heating, cooling, and second heating, in order to distinguish curie temperatures. It was found that the crystallization points and Curie temperatures in the mixed polymers were slightly lower than those of the pure components. Moreover, they compared the enthalpy and thermal properties from the different DSC tests. As the PVDF-TrFE increased, the β-phase content calculated from FT-IR spectra (assisted with XRD) and the ferroelectric property (remnant polarization) witnessed an increasing trend, where this increasement was beyond the rule of mixture. The morphology characterized by SEM showed more preferred crystalline orientation as the PVDF-TrFE weight ratio increased. Also, higher dielectric permittivity was found in the blended polymers. Therefore, Meng et al. concluded that there was strong interfacial polarization between the PVDF and PVDF-TrFE, improving the kinetics of crystallization and formation of favored crystalline structures of this polymer blend [27]. Nonetheless, this work majorly focused on the theoretical analysis and characterization, providing a bright outlook for further applications.

Suresh et al. used both solution casting and extrusion method to blend PVDF/PVDF-TrFE. Systematic characterization work was done in terms of morphology, thermal and ferroelectric properties of this polymer blend. In comparison to work of Meng et al. [27] and Jia et al. [35], mechanical properties of melt-mixed and solution-mixed PVDF/PVDF-TrFE were investigated, including elastic modulus and hardness, where the PVDF-TrFE weight percentage ranged from 0 to 100wt.% at a step of 10wt.%. As the PVDF-TrFE content increased, the elastic modulus of melt-mixed PVDF/PVDF-TrFE remained at the same level (similar trend for hardness), while the

one for solution-mixed samples decreased [38]. Nonetheless, the comparison on ultimate tensile strength among the samples was not carried out. Further applications in sensor, actuator and transducer areas remained to be investigated.

1.6. PVDF and PVDF-TrFE in sensor applications

There are a number of scientific papers investigating either PVDF or PVDF-TrFE for sensor applications.

1.6.1. Fabrication methods and corresponding results

According to Soin et al., spin-coating was efficient to fabricate ultrathin PVDF and PVDF-TrFE films. In comparison to PVDF films fabricated by melting, the samples prepared by spin coating are able to form primary β-phase instead of dominated α-phase. Therefore, spin-coating could be a valuable manufacture process to bring decent electrical output for the sensor application of piezoelectric polymers. Under designed impact tests, Soin et al. fabricated PVDF sensor, using 30wt.% PVDF spin coated with DMF at 750 rpm for 75 s. Copper film was used as the electrodes, and the sensor was encapsulated by Polyurethane (PU) for insulation and flexibility. After quenching at -20 ℃, the PVDF sensor reached an output of 3 V, which was almost three times of the value of another PVDF sensor annealed at 100℃ [39]. Badatya et al. spin coated 20wt.% PVDF with DMF at 2000 rpm for 60 s and annealed the sample at 110℃ for 5 hrs. 75% β-phase content was found in the PVDF layer. Thereafter, the PVDF film was combined with washed and dried eggshell to form layered piezoelectric membrane. Indium Tin Oxide (ITO) was selected as the electrode material and the sensor was encapsulated by Polyethylene terephthalate (PET). The non-poled sensor showed a maximum 14 V output voltage under dynamic load test. An output of 65 V was observed in the sample after poling at 500 kV/cm for 5 hrs [40]. Huang et al. fabricated self-powered pressure sensor by spin-coating of 20wt.% PVDF-TrFE with DMF on a flat silicon wafer and inverted pyramidal mold. Aluminum was sputtered on the PVDF film as electrode, and the sensor was packaged by Kapton film. After annealing at 140 ℃ for 5 min, the samples were put under a cyclic compression load test using a magnetic shaker. A maximum peak-to-peak 1.4 V output voltage was observed in the pyramidal sample while only 0.15 V was seen in the flat one [41].

1.6.2. Solvent

According to Nishiyama et al., increasing the dipole moment of the solvent might improve transformation from α- to β-phase in PVDF [42]. Among the common organic solvents, DMF was widely used for dissolving PVDF, with strong solubility and high dipole moment. Therefore, DMF was regarded as the major dipolar aprotic solvents for PVDF and its copolymers [41]. In summary, using DMF to dissolve blended PVDF/PVDF-TrFE for spin-coating was thought to be a suitable way to efficiently produce thin films for characterization and sensor fabrication.

1.6.3. Electrode and packaging material

For the fabrication of piezoelectric sensors, in order to minimize charge leakage and keep a good output electrical signal, it is essential to consider the appropriate electrode and packaging materials in sensor fabrication. Indium Tin Oxide [34], Silver [10] and Gold [11] are highly conductive but expensive electrode materials. Aluminum [41] and Copper [39] are more economic and they can be applied in large production. The conductivity of Cu and Al is usually enough for general sensor application. In order to improve the connection of the short-circuit sensor, different manufacture methods were used to produce thin electrodes on PVDF or PVDF-TrFE film, including electron beam [43], sputtering [41], or physical vapor deposition (PVD) [44]. Otherwise, direct spin coating of PVDF on thin-film electrode material is a faster and more economical method. Conventional packaging materials provide adhesion, thin thickness and electrical insulation in flexible sensor fabrication. PET [34] and Kapton film [35] are the common encapsulation materials in flexible sensor fabrication. Some packaging materials may provide additional properties to the sensor, for example, PU can bring the high flexibility and shape memory [39]. In this thesis, direct spin-coating PVDF/PVDF-TrFE on the Copper or Aluminum thin-film electrode with Kapton tape encapsulation was regarded as a feasible and economic way in PVDF/PVDF-TrFE sensor application.

To summarize this literature review section, the gap within the aforementioned work was that they only focused on morphological analysis and other characterization towards the effect of PVDF-TrFE weight ratios of blended PVDF/PVDF-TrFE. However, attempts on producing blended PVDF/PVDF-TrFE sensor remained to be done. Furthermore, the factors might influence the electrical outputs of fabricated sensors was left to be investigated. This thesis is aimed to close that gap in the literature by producing PVDF/PVDF-TrFE samples with spin-coating method and conducting customized pendulum impact tests and FT-IR characterization. These

tests are targeted to investigate the effect of PVDF-TrFE weight ratios and type of treatment (thermal and electrical) on the output voltage, sensitivity and corresponding β-phase content of the fabricated sensors.

Chapter 2. Material and Methodology

2.1. Materials

PVDF pellets (CAS number: 24937-79-9) was purchased from Sigma Aldrich. Molecular weight (Mw), density, and melting temperature of this material were reported to be 275K Dalton, 1.78g/cm^2, and 166-170℃, respectively. Solvene 250/P300 PVDF-TrFE powder was purchased from Solvay company which consists of 25 mol% of TrFE and 75 mol % of VDF. Molecular weight, density, and melting point of this material is 300K Dalton, 1.7 g/cm^2 and 146℃, respectively. The solvent for dissolving the PVDF/PVDF-TrFE was N, N-dimethylformamide (DMF) (CAS number: 68-12-2; anhydrous 99.8% purchased from Sigma Aldrich). In the extrusion and spin-coating experiments, PVDF pellets were blended with five different weight ratios of PVDF-TrFE powder as listed in Table 2.1.

Table 2.1. Weight percent of blended PVDF/PVDF-TrFE.

Designation	PVDF (wt.%)	PVDF-TrFE (wt.%)
PVDF	100	0
90/10	90	10
80/20	80	20
70/30	70	30
PVDF-TrFE	0	100

2.2. Extrusion

The extrusion process was done using a single-screw MAHOR.XYZ™ V4 pellets mini-extruder that was capable of producing small diameter filament. As such, the minimum feeding mass of PVDF was approximately 0.5g. As shown in Figure 2.1, the single-screw Mini-extruder consisted of a stainless-steel screw, copper barrel, 3D-printed hopper and a nozzle with 0.8 mm diameter (replaceable). The controller system consisted of a heating unit, a stepper motor unit, and a two-fan unit which were all controlled by Arduino software. The whole system was powered by a 24 V DC power supply. Specifically, the upper fan was attached to the hopper to ensure the pellets to remain solid state at hopper and the lower fan was to accelerate the solidification of the filament out of the nozzle and to optimize the PID temperature control. The

heating control unit included a PID temperature controller, a 40A DC to DC SSR relay to switch the high DC voltage in thermocouple using lower DC voltage in temperature controller, and a K-type thermocouple to heat the nozzle.

The filaments were extruded at 220 ℃. Although the melting points of both polymers were lower than this temperature, it was the minimum experimental heating temperature to ensure the melts of the polymer blends can flow smoothly to avoid clogging. The pulse width modulation (PWM) of stepper motor was set to be 20 in Arduino to control the rotational speed. At the beginning of the extrusion, the PWM was set to be 50 representing a lower rotational speed to warm up the system and avoid mechanism failure. Thereafter, the filaments were formed naturally under gravitational force. The diameters of the extruded filaments ranged from 1.04 mm to 1.43 mm.
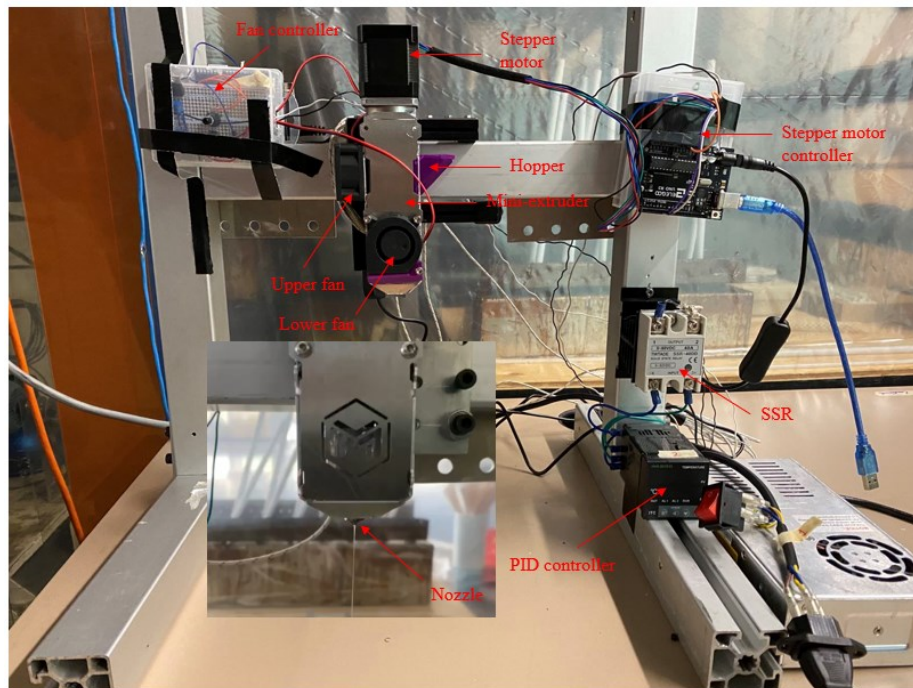
Figure 2.1. The mini-extruder operating system.

2.3. Tensile test

The tensile tests were carried out by using Electroforce 3200 Series III (as shown in Figure 2.2) with a 450 N load cell. The tests were conducted at the ambient temperature (approximately 21℃). In order to ensure the consistency of filament test without any unwanted slip or slid, firstly, the diameter of the tested filament should reach at least around 1 mm to fit the grip. Secondly,

specimens should be clamped and tightened exactly at the space between the middle tooth of the upper grip and the two corresponding teeth of the lower grip. For each sample, length was cut into 75 mm and diameter of the filament was controlled at 1.22±0.09 mm. The effective gauge length was set to be 50 mm, elongated displacement was 12mm, and the tensile rate is 6 mm/minute.

(a)   (b)
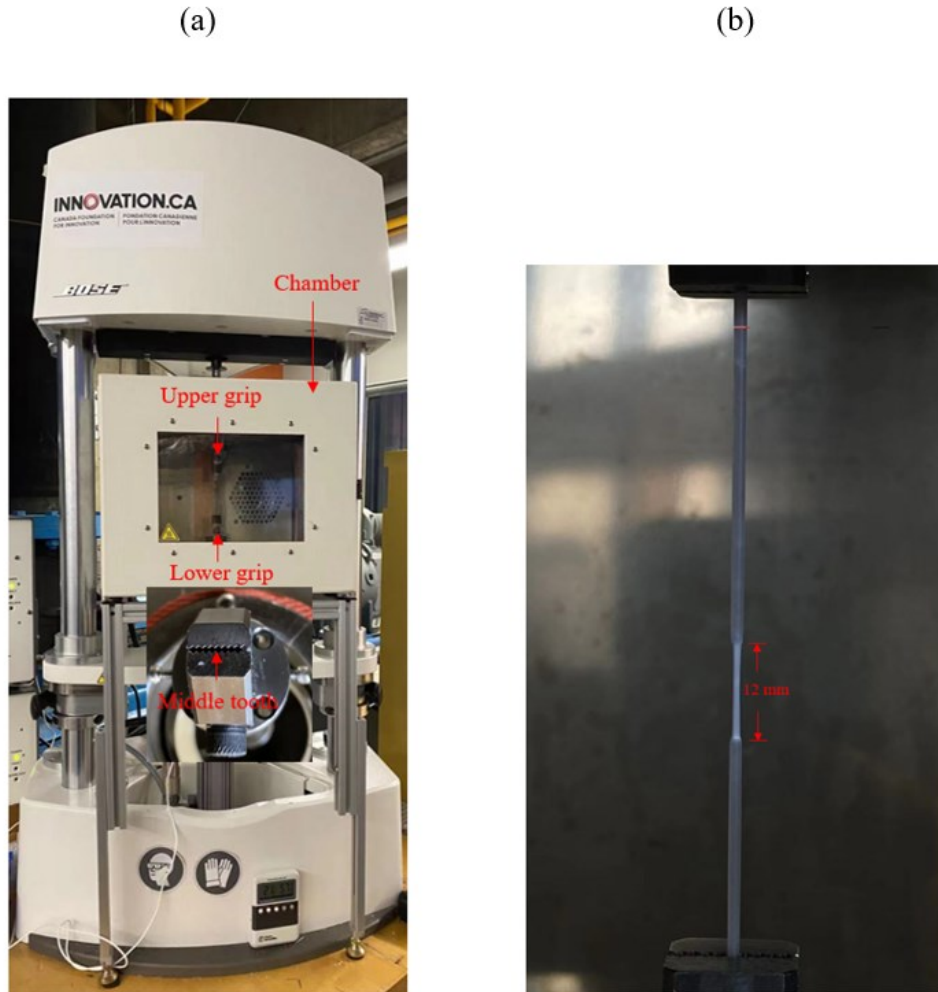
Figure 2.2. Image of (a) Electroforce 3200 Series III (b) a PVDF filament after the tensile test

The strains were calculated based on displacement (Δl) data and the effective gauge length (l) according to Eqn. (2.1),

$$\varepsilon = \frac{\Delta l}{l} \qquad (2.1)$$

The nominal stresses were obtained by the Eqn. (2.2), where F was the recorded forced and A_o was the original cross-section area of the filaments.

$$\sigma = \frac{F}{A_o} \qquad\qquad (2.2)$$

The stress-strain curves were plotted, and the elastic modulus were calculated in the linear region of the curve by using EXCEL. The ultimate tensile strength (UTS) of each teste filament could be observed based on the stress and strain curve.

For each PVDF/PVDF-TrFE weight ratio (PVDF, 90/10, 80/20, 70/30 and PVDF-TrFE), six filament samples were prepared. Half of the samples (15 out of 30) were annealed at 120 ° C for 2 hours in advance. Tests were performed in triplets for each PVDF/PVDF-TrFE concentration, and the average values are calculated and reported.

2.4. Spin coating

30wt.% of blended PVDF/PVDF-TrFE was dissolved in DMF by using magnetic stirrer at 750 rpm for 12 hrs at 20 °C and heated at 70 °C for one hr. The copper tape (substrate) was attached onto a glass slide in advance. Before the spin-coating, the glass slide was attached onto the metallic platform of the spin-coater. To start the spin-coater, the vacuum tube should be open, and the metallic platform was tightly attached onto the motor shaft inside the spin-coater. For safety consideration, aluminum foils were used to protect the cylindrical chamber from solution splash, and the whole spin-coating process was operated in a fume hood. Then an approximately 1.5 ml of blended polymer solution was deposited on the adhesive side of a copper tape substrate and spin coated at 2000 rpm for 35 seconds. For the settings by control panel, the first 5 seconds were to reach 2000 rpm and the rest of 30 seconds for film formation. The thickness of the samples was maintained at 0.032±0.005 mm. A picture of the spin coater SPINCOATER MODEL P6700 and the spin-coated samples is shown in Figure 2.3 (a) and (b) respectively.
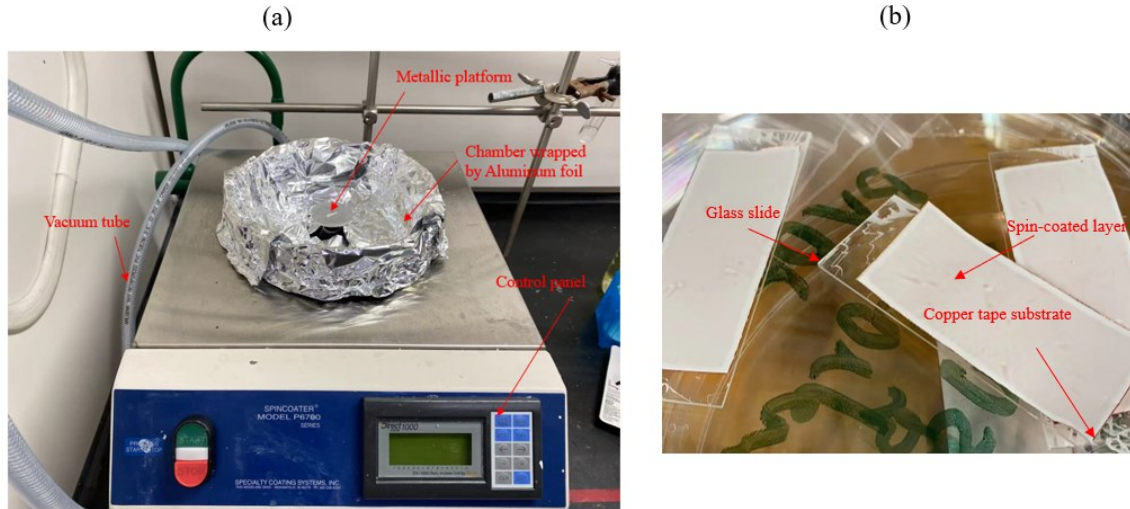
Figure 2.3. Image of (a) SPINCOATER MODEL P6700 (b) Spin-coated samples

2.5. Annealing and poling

As mentioned in the literature review, annealing and poling process was able to optimize the crystalline structure of the blended PVDF/PVDF-TrFE and may improve the piezoelectric performance of the fabricated sensors. In order to differentiate the effect of annealing and poling treatment (heating or not), the spin-coated samples at each PVDF/PVDF-TrFE ratio were divided into six groups including: No treatment, annealing, poling, poling heating, annealing poling, and annealing poling heating. For each group, there were three samples, with 90 samples in total. For the annealing process, the samples were heated at 110 ° C for 0.5 hr in the Thermo Scientific™ Lindberg/Blue M™ Vacuum Oven as shown in Figure 2.4 (a).

For the contact poling process, the samples were electrically poled under 1.5 kV (approximately 40 MV/µm) by Gamma™ High Voltage Supply. The contact poling set up consisted of an 3D printed insulation chamber, a needle electrode, a high voltage supply, a copper electrode at the bottom and a heating unit where a 3D printed layer with an insulation film was applied between copper electrode and the heating unit as shown in Figure 2.4 (b). The display screen on the left-hand side of the high voltage supply is the current in microamps through the sample, while the other one was the voltage in kilovolts. It was noticeable that despite all samples were under 1.5 kV, the current through PVDF was nearly at zero as shown in Figure 2.4 (b), while the current through PVDF-TrFE was observed to change from 3 to 9 microamps in Figure 2.4 (c), indicating the higher dielectric properties of PVDF and the better electroactivity of

PVDF-TrFE. Samples requiring annealing poling were annealed and poled afterwards. For the heating process during contact poling, the temperature was set to be 80℃.
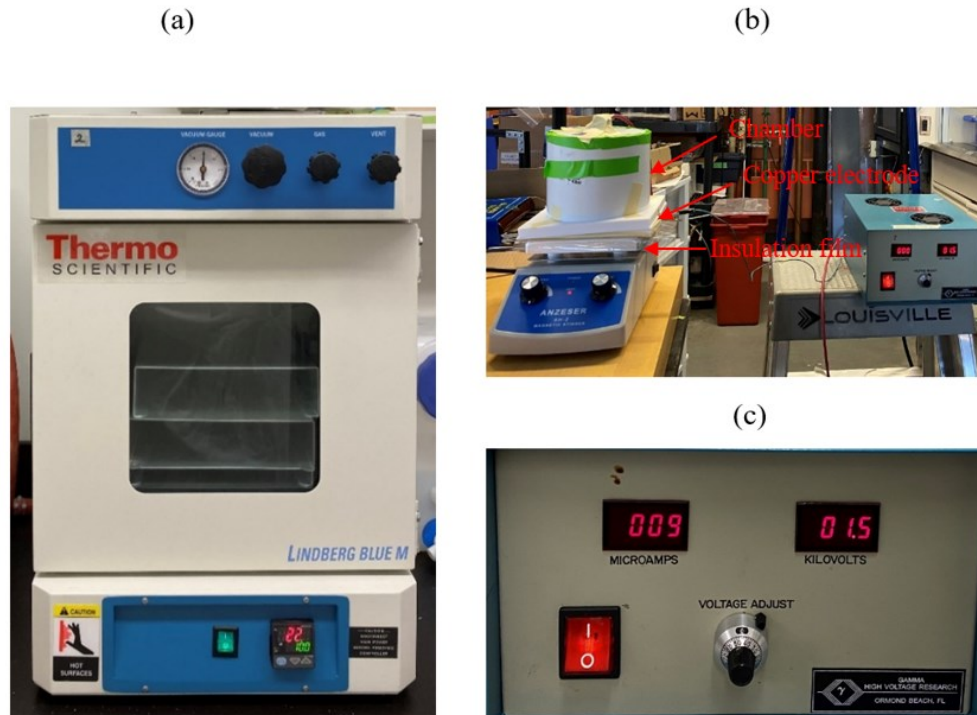
Figure 2.4. (a) Contact poling set-up. (PVDF spin-coated sample) (b) Image of Scientific™ Lindberg/Blue M™ Vacuum Oven (c) Current and voltage display through PVDF-TrFE sample.

2.6. Pendulum impact test

2.6.1. Impact sensor fabrication

In the spin-coating process, one side of the PVDF/PVDF-TrFE film was deposited on the copper tape electrode. During fabrication, the opposite side of the film was attached to another copper tape. Thereafter, the aluminum foil worked as a conductive channel which was connected to the copper electrode on each side. Finally, two Kapton tapes were used to encapsulate the inner piezoelectric polymers, electrodes, and the whole electric circuit for the charge insulation purpose. Figure 2.5 (a) and (b) presents the image of a completed sensor and its schematic view showing the different layers. The size of the sample was cut into a squared thin film with the side length (*L*) of 25 mm in order to provide large enough impact area for the following pendulum impact test.

(b)
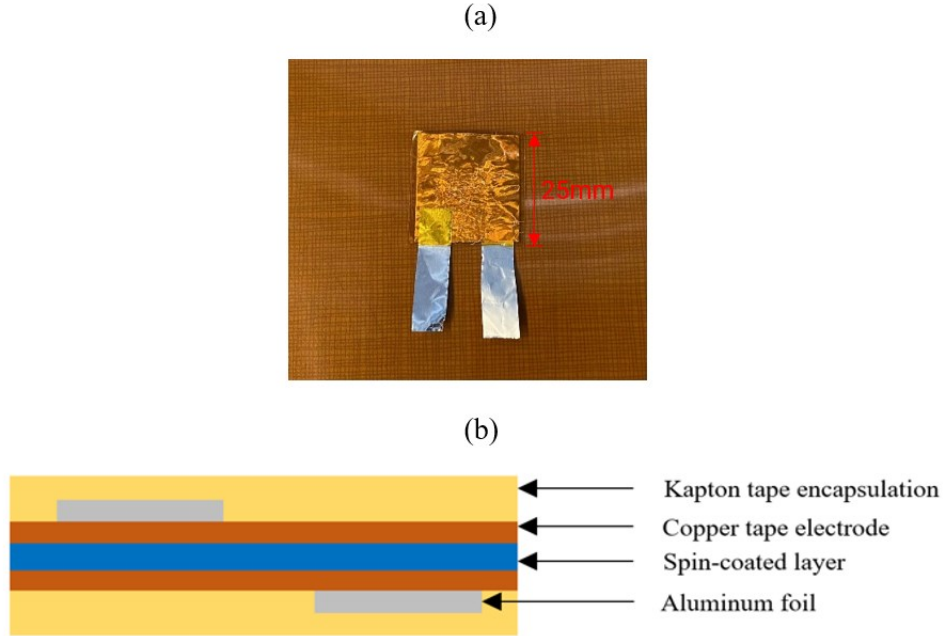
Figure 2.5. The picture of (a) an impact sensor (b) its schematic view showing the layers.

2.6.2. Pendulum impact test design and calculation

A pendulum impact test was designed and set up to provide repeatable mechanical impact on piezoelectric sensor. By considering the five concentrations and six treatments combinations, each of the total 90 samples was tested for at least three times. As shown in Figure 2.6 (b) and (c), two wood square bars were fixed on a plate, a steel ball was connected by a string to the top of the taller wood bar and held by a clip supported by the shorter wood bar. The length of the string (L_s) is 120 mm and the mass (M) and radius (R) of the steel ball is 33.071g and 10 mm respectively.

For each pendulum test, the steel ball was released by the clip and swing freely until it hits the impact sensor. The schematic area of impact within the square impact sensor is shown in Figure 2.6 (a). Figure 2.6 (b) shows the initial angle (θ_1) between the string and the taller wood bar before the steel ball is released. Figure 2.6 (c) shows the highest rebound angle (θ_2) after the first impact. These two angles were captured and recorded by a digital camera for each test. In order to calculate the speeds of the steel ball before (v_1) and after (v_2) the impact and the average force (F_{ave}) applied on the impact sensor, Eqn. (2.3) and (2.4) were used. Herein, g is the gravitational acceleration and Δt is the impact duration indicated by the oscilloscope (Tektronix 2024B).
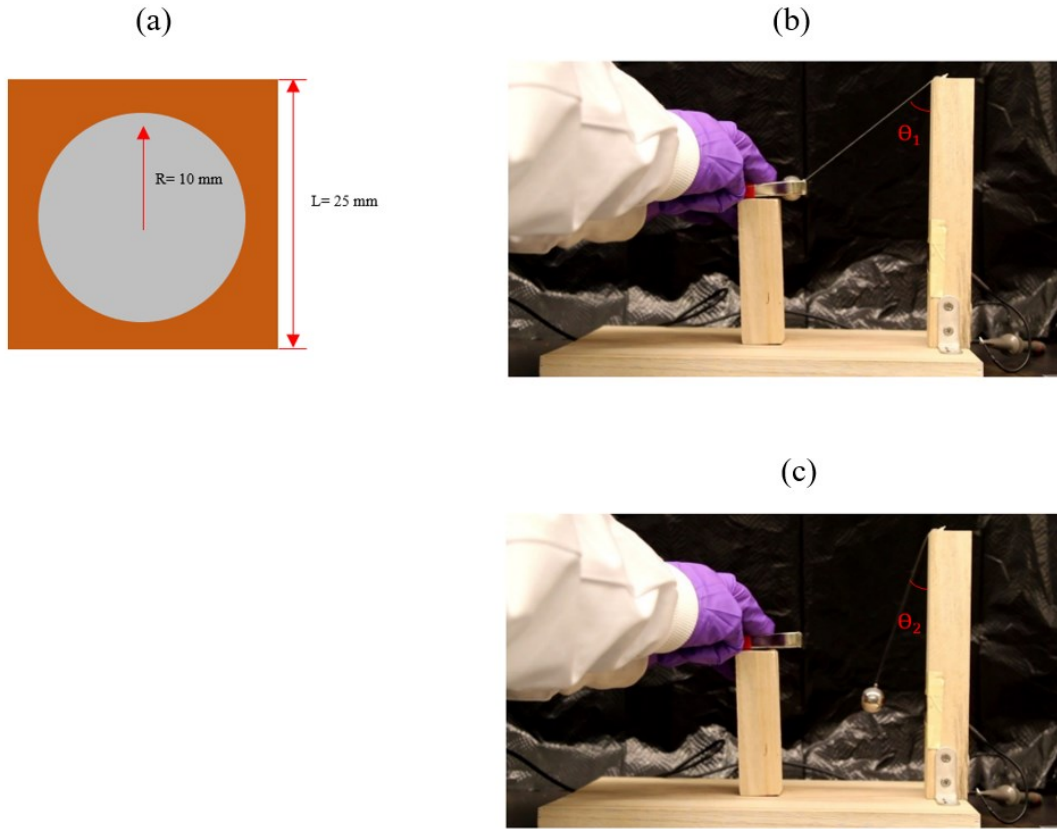
Figure 2.6. (a) Schematic view of impact area (b) Pendulum impact test at the initial angle θ_1 (c) Pendulum impact test at the rebound angle θ_2.

$$v_i = \sqrt{2g(L_S - L_s cos\theta_i)}(i = 1 \ and \ 2) \qquad (2.3)$$

$$F_{ave} = \frac{m(v_1 + v_2)}{\Delta t} \qquad (2.4)$$

In the measurement of output voltage, as shown in Figure 2.7, the two aluminum foils on the sensor were clamped by an alligator electrical clip and the oscilloscope probe respectively, where the alligator clip was attached to the grounded point of the probe. During the test, the electrodes were closely clamped by the alligator clip and probe. Thereafter, the output voltage versus time data from the impact sensor was recorded by the oscilloscope and the data was

captured and exported by using the OpenChoiceDesktop (Tektronix) software. Before the voltage measurement, the Oscilloscope was calibrated in the Autoset Mode and then set to the Measure Mode where the time interval recorded was set to be 200 ms. Also, the Glitch Capture Mode (also called Peak Detect Mode) was turned on to provide more sensitive measurement for capturing the maximum positive and negative peaks.

Figure 2.7. An image showing the connection between a sensor and the probe of oscilloscope.

Figure 2.8 shows an example of the voltage-time graph demonstrating the piezoelectric response of the PVDF/PVDF-TrFE sample upon impact. Prior to 1.1624 s, the graph shows fluctuations between -0.04 V and 0.04 V, which corresponded to noise in the oscilloscope. At 1.1624 s (the first impact), the first prominent peak (0.32 V) appeared, followed by a drop in signal to -0.64 V at 1.1636 s (see zoom-in view on the right of Figure 2.8). After a few relatively large increases and decreases in the signal, the graph returned to small fluctuations (noise) at 1.1671 s and lasted until the second impact at 1.4712 s. During the first impact, the maximum positive peak (hereafter denoted as V_{pm}) is 0.32 V at 1.1624 s, while the maximum negative peak (hereafter denoted as V_{nm}) is -0.64 V at 1.1636 s. The peaks became smaller in the subsequent impacts due to energy dissipated in the pendulum's motion. The V_{pm} and V_{nm} was recorded as the electrical outputs of the first impact (magnitude and direction) for further analysis. According to Eqn. (2.5), the difference between V_{pm} and V_{nm} was denoted as peak-to-peak voltage (V_{pk-pk}). To calculate F_{ave} in the aforementioned Eqn. (2.4), Δt was also defined as the time difference between V_{pm} and V_{nm}. For example, as shown in the Figure 2.8, the Δt was calculated between the

1.1624 s and 1.1636 s. After calculating the F_{ave} and $V_{pk\text{-}pk}$ value of the sensor during the first impact, the sensitivity (Se) can be calculated through Eqn. (2.6).
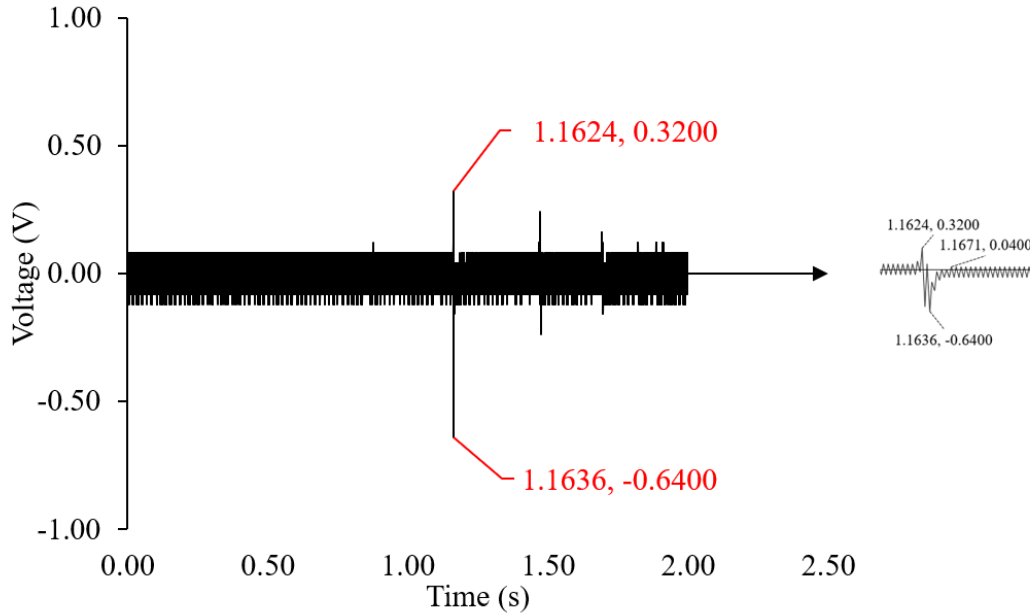
Figure 2.8. An example of voltage signal from oscilloscope used to determine V_{pm}, V_{nm}, Δt and $V_{pk\text{-}pk}$.

$$V_{pk-pk} = V_{pm} - V_{nm} \qquad (2.5)$$

$$Se = \frac{V_{pk-pk}}{F_{ave}} \qquad (2.6)$$

2.7. Characterization‑Fourier Transform Infrared Spectroscopy (FT-IR)

The six spin-coated concentrations of blended PVDF/PVDF-TrFE including pure PVDF and PVDF-TrFE were characterized by the FT-IR (Thermo Scientific™ Nicolet™ iS50). By considering the five different concentrations and six treatments mentioned above, there were 30 samples investigated and compared using FT-IR. The samples were spin-coated on a rigid copper plate substrate in order to provide an opaque background. FTIR can identify a range of functional

25

groups and the changes in molecular structure. The theory behind this is to make the samples be exposed under IR radiation, where some radiations with specific wavenumbers can penetrate the material, while some are absorbed [45] [46]. Herein, FT-IR was used to detect the existence of α, β, and γ crystalline phases in the PVDF and blended PVDF/PVDF-TrFE. The FT-IR results are fully discussed in the Section 3.3.

Chapter 3. Result and Discussion

3.1. Mechanical Properties

According to the stress-strain curves extracted from the tensile test data, the mechanical properties of the blended PVDF/PVDF-TrFE were analyzed. Due to the safety concerns of excessive voltage, electrical poling along the length direction of the filament samples was not carried out. Therefore, only the mechanical properties of untreated and annealed samples were compared. Representative stress-strain curves are shown in Figure 3.1 and Figure 3.2, for untreated and annealed samples respectively. As the PVDF-TrFE content increased, a general decrease in the level of nominal stress was observed.
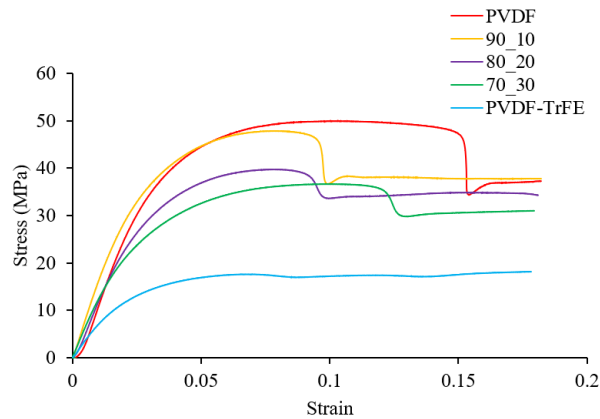
Figure 3.1. Representative stress-strain curves of untreated samples.
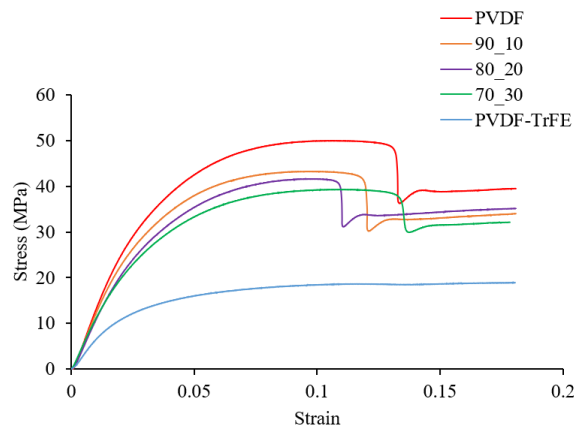
Figure 3.2. Representative stress-strain curves of annealed samples.

For PVDF and the 90/10, 80/20 and 70/30 samples, there was a sudden drop in the curve

after the stress reached the highest level, which might be due to the instability under the specified loading rate [47], where necking began as soon as yielding occurred. As shown in Figure 3.3 (a), there was a significant necking region in the PVDF filaments, and this phenomenon also took place in 90/10, 80/20 and 70/30 samples. In contrast, the stress curve of the PVDF-TrFE sample formed a plateau in the plastic region. As seen in the Figure 3.3 (b), under the same displacement, the necking in PVDF-TrFE was milder, indicating a higher ductility than PVDF. The orientated crystalline structure in PVDF-TrFE might provide more space for the polymer chains to be stretched and elongated. Nonetheless, this difference did not affect the elastic modulus calculation, which was based on the initial linear region of the stress-strain curves.

(a)   (b)
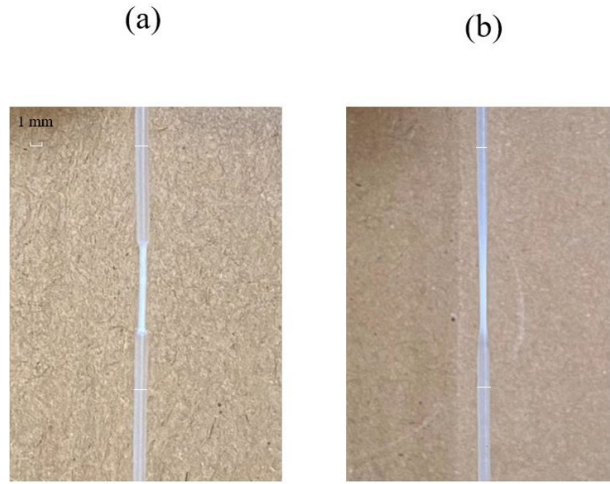
Figure 3.3. Images of filament after tensile test (a) PVDF (b) PVDF-TrFE.

Table 3.1 and Table 3.2 list the detailed information on ultimate tensile strength (UTS), elastic modulus and the diameter of the unannealed and annealed samples, as well as calculated statistics. A general rule of mixture (ROM) was used to predict the elastic modulus of the blended PVDF/PVDF-TrFE (E_{blend}) as shown in Eqn. (3.1), where f was the volume fraction of PVDF-TrFE, and E_1 and E_2 represented the elastic modulus of PVDF-TrFE and PVDF respectively. Volume fraction is used here instead of mass fraction because the density of both polymers were assumed to be 1.78 g/cm^3.

$$E_{blend} = fE_1 + (1-f)E_2 \qquad (3.1)$$

By substituting the average elastic moduli of PVDF-TrFE and PVDF into Eqn. (3.1), the calculated values for untreated and annealed 90/10, 80/20, and 70/30 samples are shown in Figure 3.4. Comparison with the experimental data in the same figure showed an excellent agreement, suggesting that the elastic modulus followed the rule of mixture.
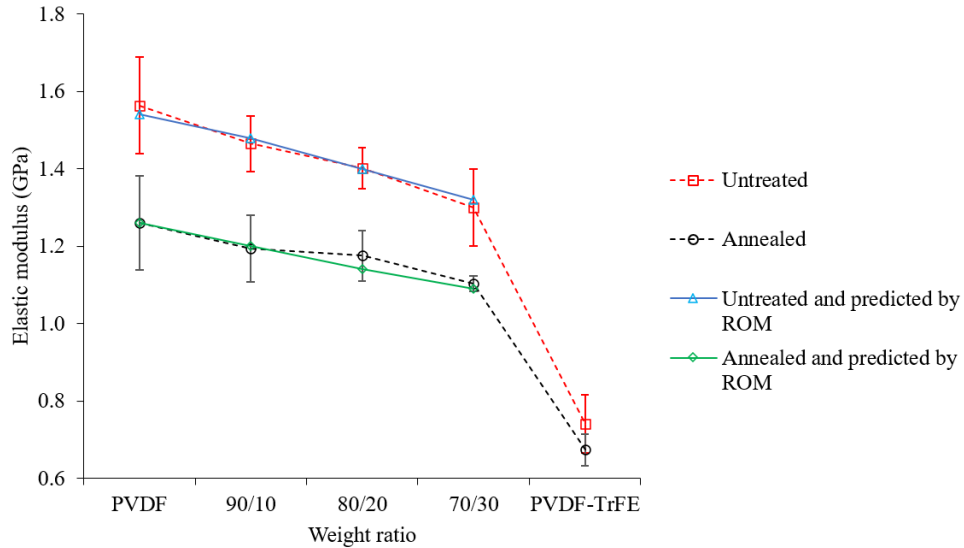
Figure 3.4. Elastic modulus at different PVDF/PVDF-TrFE weight ratios, compared with the values calculated by ROM.

Different from our results, Suresh et al. reported that the elastic modulus of melt-blended PVDF/PVDF-TrFE thin films levelled off at around 3.8 GPa as the weight fraction of PVDF-TrFE increased instead of experiencing a continuous decline [38]. At any PVDF-TrFE ratio, the elastic modulus in Suresh et al. was at a higher level than the value found in this work. The discrepancy might be due to differences in the melt-mixed procedures. Our samples were directly extruded, while sample of Suresh et al. were solution-mixed at first and then melt-mixed. Using solvent before extrusion at high temperature might introduce a larger and more uniformly distributed grain size, improving the crystallinity of the polymer blends. The free volume available for the movement of the polymer chains could be reduced, resulting in the increase of elastic modulus. In the same work, Suresh et al. also measured the elastic modulus of PVDF/PVDF-TrFE manufactured by solution mixing. A lower level of elastic modulus (from 2.5 to 1.0 GPa) was found, with a decreasing trend as the PVDF-TrFE weight ratio increased [38]. The observation was attributed to morphology changes caused by the low manufacture temperature, including vanishing grain structure, low crystallinity and poor packing of the

polymer chains.
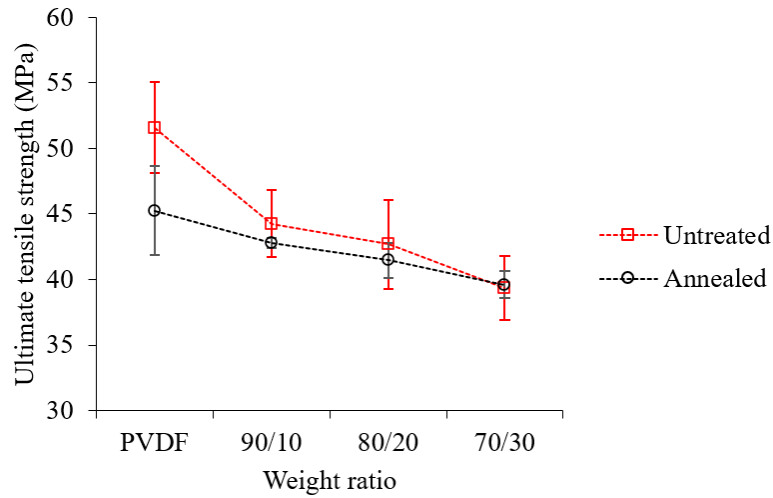
Figure 3.5. Ultimate tensile strengths at different PVDF/PVDF-TrFE weight ratios.

Figure 3.5 shows the UTS for the pure and blended polymers. As the PVDF-TrFE content increased, the UTS also decreased. Due to the limitation of the maximum vertical displacement that can be provided by the tensile test machine, the exact UTS of pure PVDF-TrFE cannot be captured. However, in Cai et al. (2017) [48] and Vatansever et al. [49], it was shown that the UTS of this pure polymer ranged from around 18 MPa to 25 MPa, which was much smaller than the value for PVDF. This UTS range also matched our maximum stress value of PVDF-TrFE during the tensile test after the curve had plateaued. Therefore, the addition of PVDF-TrFE reduced the overall UTS of the blended polymers, and this decreasing trend could be confirmed in Figure 3.1, 3.2 and 3.5. Due to the insufficient UTS data, the ROM calculation and comparison was not carried out.

As shown in Figure 3.5, the overall elastic modulus and UTS of annealed samples were at a lower level in comparison to the untreated ones. According to Buchdahl et al. [20], annealing below the melting point may cause brittleness due to spherulite formation, which could partially explain the reduction in strength and modulus after annealing. However, according to Li et al., [22], both tensile strength and elastic modulus could increase after annealing due to the crystallinity and orientation enhancement during the process, and there seems to be a conflict between the two reports. Our experimental results were in agreement with Buchdahl et al., where annealing-induced microstructure defects appeared to exceed the potential enhancement by improving crystallinity and orientation.

Table 3.1. Mechanical properties and diameters of unannealed filament samples.

Sample name	UTS (MPa)	Elastic modulus (GPa)	Average diameter (mm)
PVDF 1	51.59	1.73	1.15
PVDF 2	54.87	1.53	1.18
PVDF 3	46.44	1.43	1.2
Average	**51.59**	**1.56**	
STD	3.47	0.13	
90/10 1	47.83	1.5	1.13
90/10 2	42.75	1.36	1.16
90/10 3	42.24	1.53	1.12
Average	**44.27**	**1.47**	
STD	2.52	0.07	
80/20 1	47.43	1.48	1.15
80/20 1-2	41.01	1.36	1.15
80/20 2-2	39.66	1.37	1.24
Average	**42.7**	**1.4**	
STD	3.39	0.05	
70/30 2	36.65	1.21	1.32
70/30 3	38.91	1.25	1.38
70/30 4	42.56	1.44	1.42
Average	**39.37**	**1.3**	
STD	2.43	0.1	
PVDF-TrFE 1		0.68	1.16
PVDF-TrFE 2		0.69	1.33
PVDF-TrFE 3		0.85	1.23
Average		**0.74**	
STD		0.08	

Table 3.2. Mechanical properties and diameters of annealed filament samples.

Weight ratio	UTS (MPa)	Elastic modulus (GPa)	Average diameter (mm)
PVDF 1	49.95	1.43	1.17
PVDF 2	41.93	1.19	1.25
PVDF 3	43.87	1.16	1.3
Average	**45.25**	**1.26**	
STD	3.42	0.12	
90/10 1	42.35	1.08	1.24
90/10 2	42.74	1.2	1.33
90/10 3	43.3	1.3	1.13
Average	**42.79**	**1.19**	
STD	0.39	0.09	
80/20 1	41.64	1.2	1.12
80/20 2	39.71	1.09	1.31
80/20 3	43.02	1.24	1.24
Average	**41.46**	**1.18**	
STD	1.36	0.07	
70/30 1	38.6	1.08	1.11
70/30 2	39.25	1.12	1.14
70/30 3	40.99	1.11	1.09
Average	**39.61**	**1.1**	
STD	1.01	0.02	
PVDF-TrFE 1		0.63	1.13
PVDF-TrFE 2		0.72	1.27
PVDF-TrFE 3		0.68	1.33
Average		**0.67**	
STD		0.04	

3.2. Pendulum impact test

3.2.1. Patterns of output voltage

Based on the definition and terminology in Section 2.6.2, four different voltage patterns were observed and defined during the pendulum impact experiments, including (+;-), (-;+), (+) and (-). In the (+;-) mode, during the first impact, a maximum positive voltage (V_{pm}) appeared first, followed by a maximum negative voltage (V_{nm}). This is the mode shown in Figure 3.6, which was also reported in [39] [40]. Figure 3.7 shows an example of the (-;+) mode, where a V_{nm} signal appeared at first followed by a V_{pm}, and this mode was reported in several published papers [39] [41] [50]. In Figure 3.8, no negative peaks could be identified and only a V_{pm} appeared in the first impact, denoted by the (+) mode. The (+) mode appeared rarely in the recorded data and was not mentioned in any other literatures; thus, this mode might be caused by poor contact in a few samples. To ensure data authenticity, this mode and associated data were retained. In Figure 3.9, only a V_{nm} could be identified as a result of the first impact, and this pattern was regarded as (-) mode. This pattern was presented in Hadimani et al., as a result of impact test on commercial PVDF films [51]. Table 3.3 summarizes the frequency of occurrence of these voltage patterns for different PVDF/PVDF-TrFE weight ratios. The majority of the cases (66.3%) were categorized in the (+;-) mode, while the rest of them were mostly in (-;+) (15.6%) or (-) (17.4%) modes and only 0.7% followed the (+) mode. Although not dominating, the (-;+) mode was observed for all the weight ratios, where the majority of this mode (31.0%) were observed in the PVDF-TrFE samples. A large quantity of the 80/20 (31.5%) and 70/30 (37.0%) samples were identified as the (-) mode. It seemed that as the PVDF-TrFE weight fraction increased, the occurrence of the negative output increased. The occurrences of voltage modes under different treatments are listed in Table 3.4, the majority of (-;+) mode appeared under annealing (37.5%) and poling heating (30.0%), while the (-) mode appeared most frequently under poling heating (24.49%).

The different signs of the output voltage might originate from multiple sources. Firstly, as the stress state in the PVDF/PVDF-TrFE sample was compressive during the direct impact, intuitively the voltage response from the samples would be expected to be in one direction. On the other hand, Hu et al. reported that the PVDF-based impact sensor was equivalent to a capacitor in an open circuit. As the induced charges were generated, they would attach to the

surface of the electrodes. Because the PVDF-based film was polarized in one direction, as soon as a voltage was generated, the induced charges would immediately react in the opposite direction. Hence, their samples showed a higher negative voltage after the initial positive voltage [52]. Some argued that the negative electrical output was an inherent feature of PVDF and PVDF-TrFE. For example, the output from the d_{33} meter was always negative for these two materials, opposite to that of conventional ceramic materials [53]. However, this idea cannot explain the occurrence of positive voltage in our case. There were also hypotheses in the literature that negative response could result from the defects in the polymer structure [54].

In summary, our experimental results mainly agree with those of Hu et al. As confirmed in Figure 3.6, Figure 3.7 and the majority of the voltage-time plots in the (+;-) and (-;+) modes, the magnitude of the first peak was slightly lower than the second peak in the opposite direction, possibly due to the counteraction of the stored charges. The cause of different signs of the first peak might be the different polarization direction in each sample. The polarization was either spontaneous (for non-treated samples) or induced by thermal and electrical treatments. To explore this, the positive and grounded probes connected on the samples were swapped and impact test was repeated. While in the majority of the cases the sign of first peak reversed, not all the samples showed the sign reversal. For example, as the PVDF-TrFE content reached 20 and 30wt.% or experienced annealing and poling heating, the irreversibility of output direction appeared more frequently, which might correspond to the increased portion of defects in the material structure.
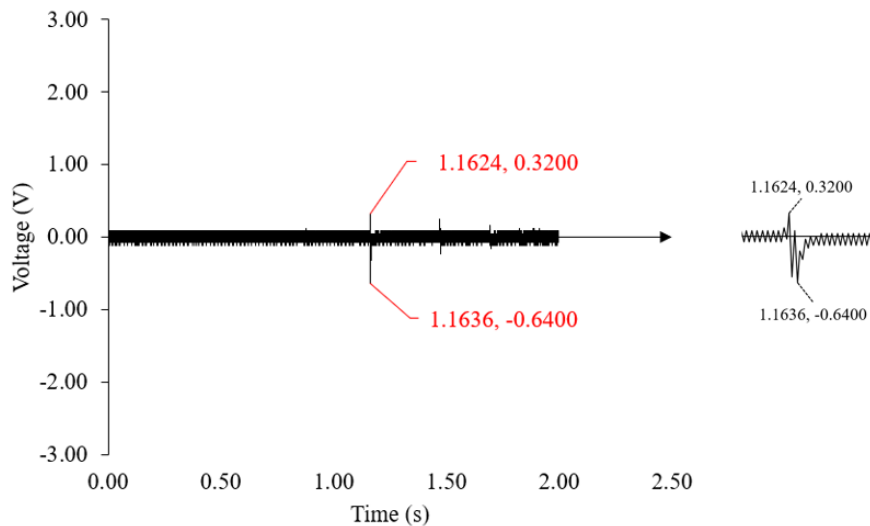
Figure 3.6. An example for the (+;-) output mode of the voltage; zoom-in view provided on the right.

34
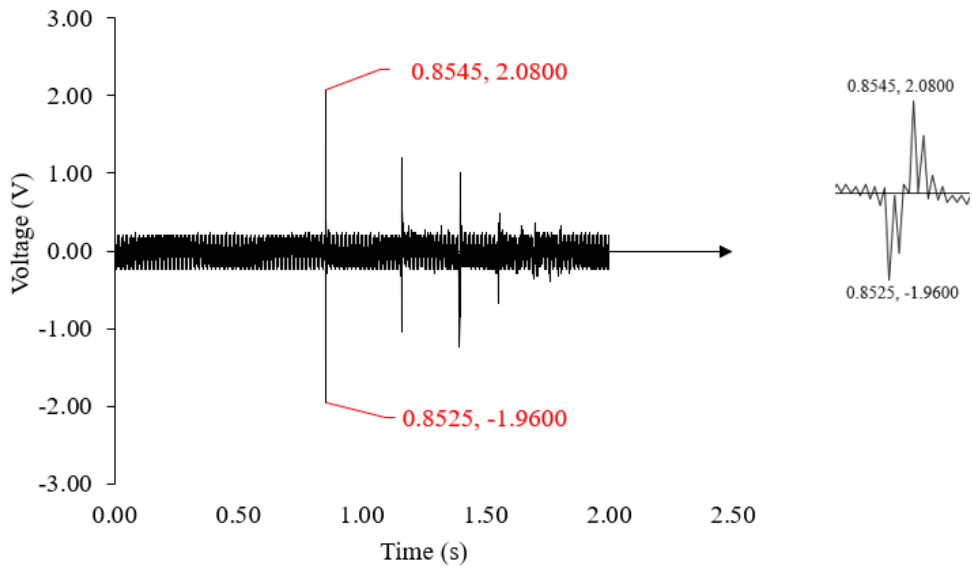
Figure 3.7. An example for the (-;+) output mode of the voltage; zoom-in view provided on the right.
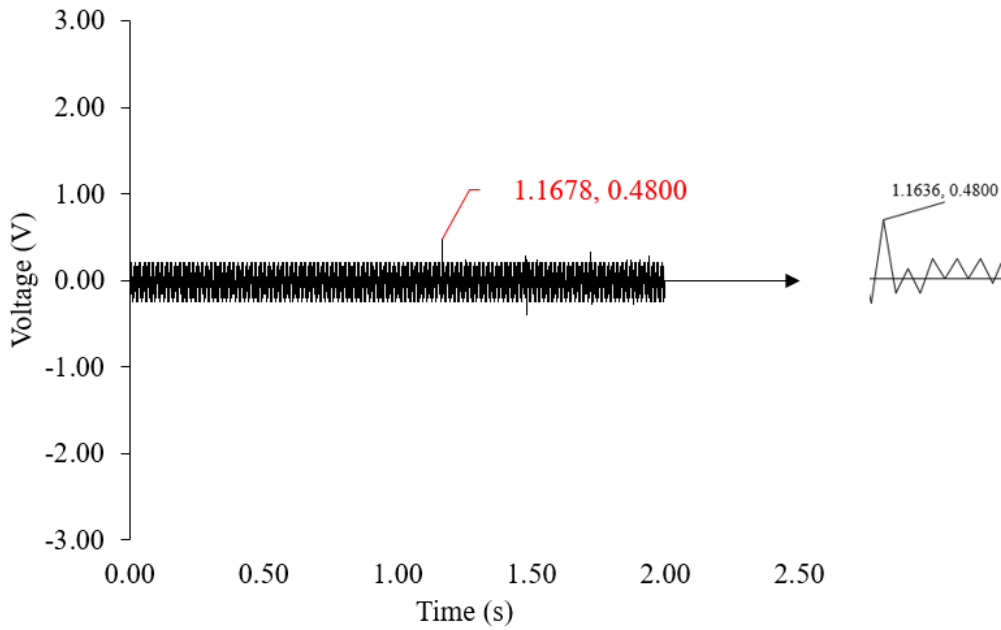
Figure 3.8. An example for the (+) output mode of the voltage; zoom-in view provided on the right.
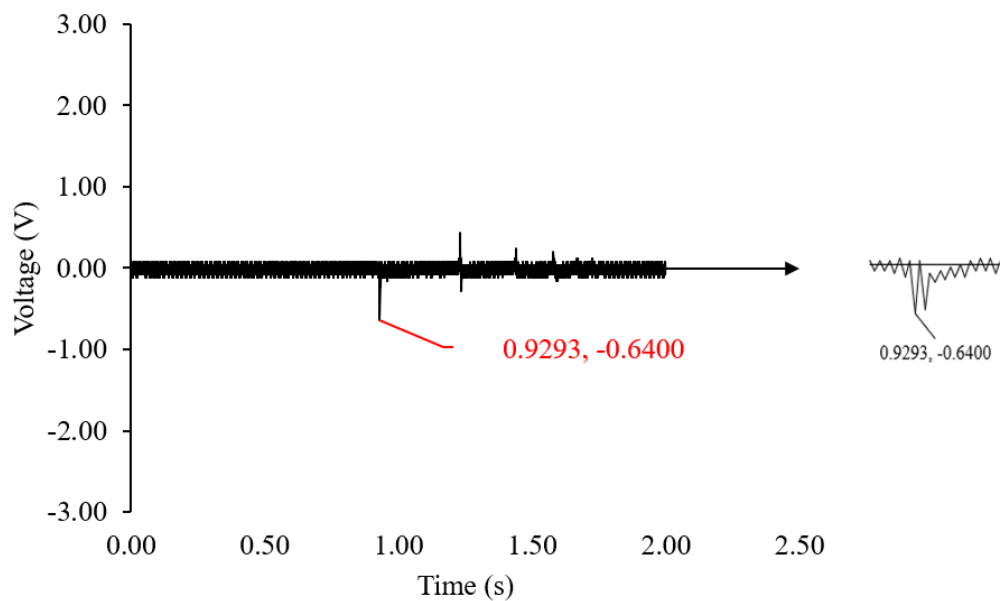
Figure 3.9. An example for the (-) output mode of the voltage; zoom-in view provided on the right.

Table 3.3. The voltage output patterns of samples. at different weight ratios.

Voltage pattern Weight ratio	(+;-)	(-;+)	(+)	(-)	Total
PVDF	44	9	0	1	54
90/10	45	8	0	1	54
80/20	27	10	0	17	54
70/30	28	2	0	24	54
PVDF-TrFE	35	13	2	4	54
Total	179	42	2	47	270

Table 3.4. The voltage output patterns of the samples under different treatments.

Treatment \ Voltage pattern	(+;-)	(-;+)	(+)	(-)	Total
No Treatment	38	1	0	6	45
Annealing	26	15	0	4	45
Poling	27	9	0	9	45
Poling heating	21	12	0	12	45
Annealing poling	36	2	0	7	45
Annealing poling heating	31	1	2	11	45
Total	179	40	2	49	270

3.2.2. Magnitude of output voltage

Figure 3.10 shows the maximum positive voltage (V_{pm}) during the first impact for all the polymers weight ratios and treatments. The pure PVDF-TrFE presented the highest V_{pm} in spite of its relatively high standard deviation, showing that PVDF-TrFE exhibited the greatest electroactive property. The second highest level of V_{pm} was observed in the weight ratio of 90/10. V_{pm} of 80/20 and 70/30 was at a much lower level than the aforementioned weight ratios. Table 3.5 shows the largest and smallest V_{pm} at any given weight ratios, as well as the corresponding treatment. Among all weight ratios and treatment methods, the pure PVDF-TrFE samples with the annealing poling treatment had the highest V_{pm} (1.39 V). The PVDF-TrFE samples under annealing or annealing poling also presented high values as shown in Figure 3.10. The largest V_{pm} for 90/10 was obtained from the samples after annealing poling (1.15V), and for the pure PVDF samples the largest V_{pm} was found from annealing poling heating treatment. Except for 80/20 and 70/30, the smallest V_{pm} all corresponded to the non-treated samples, revealing that the thermal and electrical treatments were effective in enhancing the electric output of the PVDF/PVDF-TrFE samples. Theoretically, annealing poling heating was the most integrated treatment method and expected to improve the piezoelectric response of the material. However, there was a significant drop in V_{pm} for PVDF-TrFE and 90/10 under this treatment (Figure 3.10). This might be attributed to the defects in the polymer structure induced by heating for excessive time. In contrast, there was increase in V_{pm} for PVDF after annealing poling heating, possibly resulting

from its higher melting point and resistance to heat.

Figure 3.10. Maximum positive output voltage for samples of different weight ratios and treatments.

Table 3.5. The largest and smallest V_{pm} for the samples at specific weight ratios, and the corresponding treatments.

Weight ratios	Largest V_{pm} (V)	Smallest V_{pm} (V)
PVDF	0.65 Annealing poling heating	0.23 No treatment
90/10	1.15 Annealing poling	0.36 No treatment
80/20	0.36 No treatment	0.19 V Annealing poling heating
70/30	0.36 No treatment	0.12 poling
PVDF-TrFE	**1.39 Annealing poling**	0.23 No treatment

Figure 3.11 shows the maximum negative voltage (V_{nm}) during the first impact for all the polymers with different weight ratios and treatments. The pure PVDF-TrFE still produced the strongest V_{nm} signals, while the 90/10 samples showed the second highest level. 70/30 showed a decent voltage performance, which had little variation with the treatment. V_{nm} of 80/20 was moderate, and PVDF presented the lowest V_{nm}. Table 3.6 shows V_{nm} of the largest and smallest

magnitude at any given weight ratio, as well as the corresponding treatment. Among all weight ratios and treatment methods, the PVDF sample showed the smallest magnitude of V_{nm} under no treatment (-0.28 V). In contrast, PVDF samples under annealing poling heating reached -0.87 V, demonstrating a significant response of PVDF towards the electrical and thermal treatment. However, the largest magnitude of V_{nm} occurred in the 90/10 samples under annealing poling (-1.76 V), indicating the superior electroactivity at this weight ratio of blending. The 80/20 samples obtained its largest V_{nm} magnitude after poling, while the 70/30 samples showed its greatest V_{nm} magnitude with no treatment. The largest magnitude of V_{nm} among PVDF-TrFE samples was found under annealing and poling (-1.43 V).
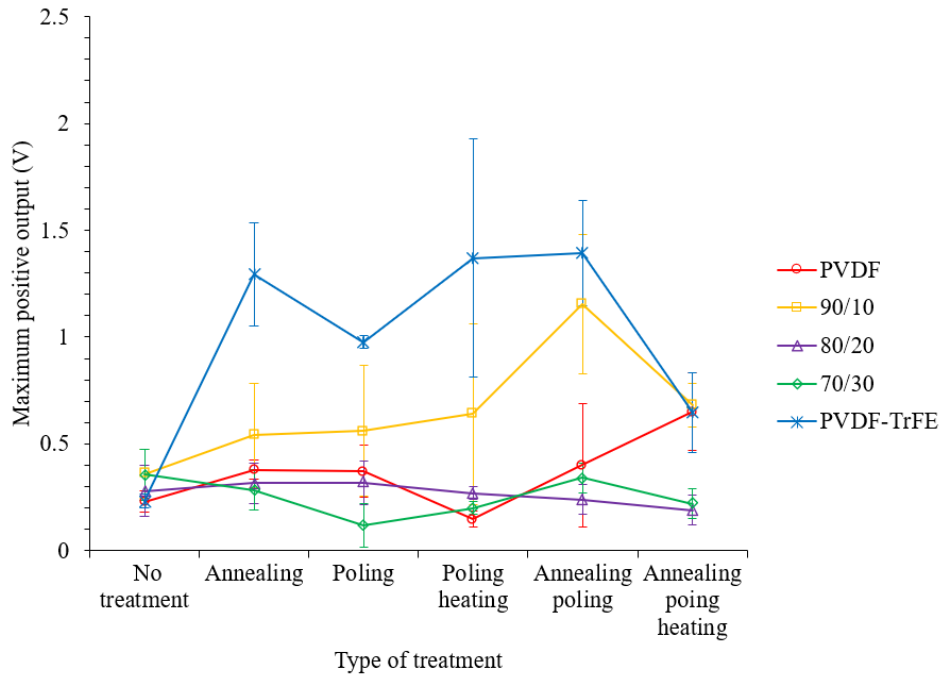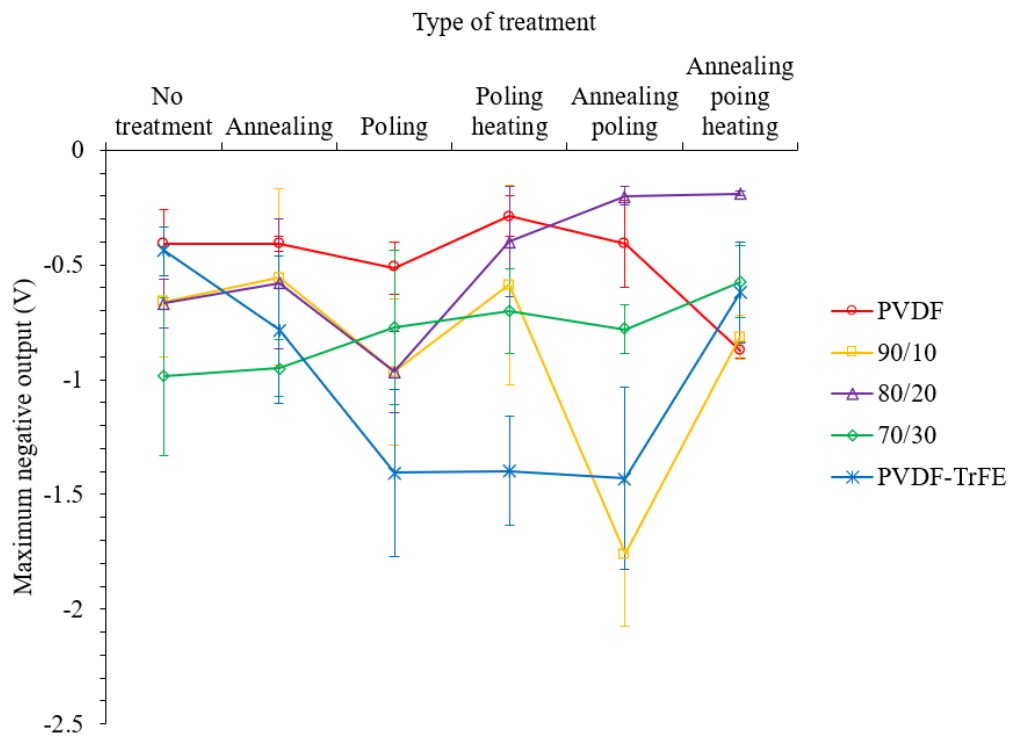

Figure 3.11. Maximum negative output voltage for samples of different weight ratios and treatments.

Table 3.6. V_{nm} with largest and smallest magnitude for the samples at specific weight ratios, and the corresponding treatments.

Weight ratios	V_{nm} of largest magnitude (V)	V_{nm} of smallest magnitude (V)
PVDF	-0.87 Annealing poling heating	-0.28 No treatment
90/10	**<u>-1.76 Annealing poling</u>**	-0.55 Annealing
80/20	-0.96 Poling	-0.19 Annealing poling heating
70/30	-0.95 Annealing	-0.57 Annealing poling heating
PVDF-TrFE	-1.43 Annealing poling	-0.44 No treatment

3.2.3. Sensitivity analysis

According to Eqn. (2.3), the average force (F_{ave}) was calculated based on v_1 and v_2 (speeds of the steel ball before and after impact) as well as the impact duration (Δt). According to Eqn. (2.5), the peak-to-peak voltage (V_{pk-pk}) was calculated using the highest positive peak (V_{pm}) and the lowest negative peak (V_{pm}). By substituting V_{pk-pk} and F_{ave} into Eqn. (2.6), the resultant sensitivity (Se) was calculated. As the Δt of (+) or (-) mode could not be determined based on this peak-to-peak method, these two modes were not considered in the Se analysis. Figure 3.12 shows V_{pk-pk} for all polymers with different weight ratios and treatments. PVDF-TrFE had the highest level in V_{pk-pk}, followed by 90/10, 70/30, 80/20 and PVDF respectively. Table 3.7 shows the largest and smallest V_{pk-pk} at any given weight ratio, as well as the corresponding treatment. Among all weight ratios and treatments, 90/10 samples under annealing poling presented the largest V_{pk-pk} (2.91 V). The smallest V_{pk-pk} was found in 80/20 under annealing poling heating (0.38 V).
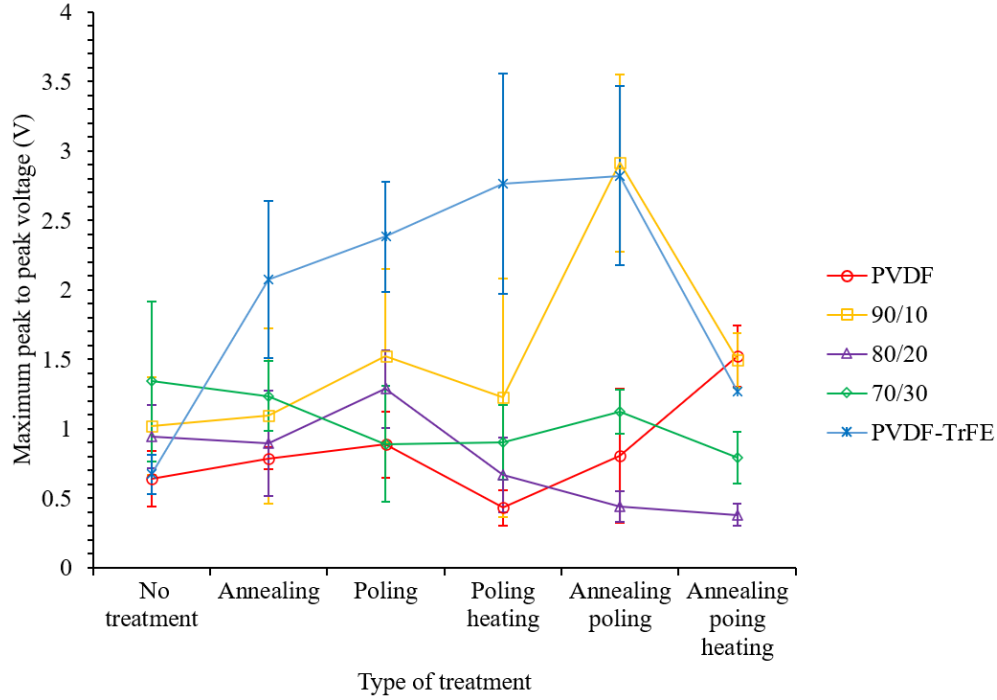
Figure 3.12. Peak-to-peak voltage for samples of different weight ratios and treatments.

Table 3.7. The largest and smallest $V_{\text{pk-pk}}$ for the samples at specific weight ratios, and the corresponding treatments.

Weight ratios	Largest $V_{\text{pk-pk}}$	Smallest $V_{\text{pk-pk}}$
PVDF	1.52 V Annealing poling heating	0.64 V No treatment
90/10	**2.91 V Annealing poling**	1.02 V No treatment
80/20	1.03 V poling	0.38 V Annealing poling heating
70/30	1.34 V No treatment	0.79 V Annealing poling heating
PVDF-TrFE	2.82 V Annealing poling	0.67 V No treatment

Figure 3.13 shows the sensitivity (Se) for all polymers with different weight ratios and treatments. The ranking of Se generally followed the same trend in $V_{\text{pk-pk}}$, although Se of PVDF surpassed 80/20 and 70/30, reaching the third highest. For each weight ratio, 18 samples were divided into six groups, one for a particular type of treatment, and each treatment was tested in triplets. The initial angle (θ_1) was controlled in the tests and therefore almost the same for all samples. The rebound angle (θ_2) angle was also found to be consistent in the repetitive tests. Therefore, for each treatment at a given weight ratio, one representative sample was selected (out

41

of the three) for data presentation. Table 3.8 shows the θ_1 and θ_2 angles, as well as F_{ave} for the representative samples at different weight ratios. Figure 3.14 compares the statistics of θ_2 of the representative samples. The standard deviation among the six different treatments was negligibly small, and the values in Table 3.8 were calculated from the average of the representative samples under each weight ratio. θ_2 was significantly smaller than θ_1, suggesting that a considerable fraction of the steel ball's kinetic energy just before the impact was either converted to electrical energy by the sample, or dissipated in the form of heat. Since F_{ave} was proportional to the velocity of the steel ball after impact (v_2), higher F_{ave} and θ_2 corresponded to larger kinetic energy of the ball after impact. As the PVDF-TrFE content increased, an increasing trend in θ_2 could be observed in Figure 3.14, suggesting less conversion to electrical energy and heat. However, Se did not follow the same trend. Pure PVDF-TrFE and 90/10 had the highest Se, suggesting that they were more effective in converting the kinetic energy into electrical energy (k_{33}) and reducing dissipation caused by heat. For 70/30 and 80/20, their Se was lower even than pure PVDF, indicating more kinetic energy was converted into heat instead of electrical energy.

As described by Hu et al., there is an intrinsic energy barrier associated with the crystal nucleation and chain mobility of polymeric materials [55]. Jia et al. reported that as the PVDF-TrFE content increased from 10 to 50wt.%, this energy barrier increased in PVDF/PVDF-TrFE [35]. Su et al. proposed that higher energy barrier implied that the dipole moment was more difficult to be oriented by external stress or electrical field. In other words, for the samples with higher energy barrier, a larger threshold stress is required to generate the specified electrical output [56]. In our experiments, as the PVDF-TrFE content increased from 10 to 30wt.%, the PVDF and PVDF-TrFE chains might become more entangled near the immiscible interfaces leading to decreased chain mobility. Therefore, the threshold stress tended to be high, and the electrical output and corresponding Se were at a lower level under the same mechanical impact. Within this range of weight ratios, the immiscible PVDF/PVDF-TrFE might experience higher heating dissipation than the single-phase pure components due to the presence of interfaces. A low fraction (10wt.%) of PVDF-TrFE, the chain entanglement was not significant and did not cause large impact on the chain mobility. Therefore, the electroactivity brought by PVDF-TrFE might exceed the interfacial energy dissipation, resulting in higher Se than PVDF, 70/30 and 80/20. According to Jia et al., after the PVDF-TrFE content reached 50wt.%, the dominant PVDF-TrFE drastically improved the β-phase content of the solution-mixed PVDF/PVDF-TrFE

[35]. Yu et al., using a quantitative method, found that the energy barrier for dipole moment flipping experienced a sudden drop at 50wt.% of PVDF-TrFE. These literatures revealed the potential enhancement of performance beyond this weight ratio [57]. However, 50/50 was not attempted in our sensor fabrication due to the cost consideration.

Table 3.9 shows the largest and smallest Se at any given weight ratio, as well as the corresponding treatment. The largest Se among all samples occurred in the 90/10 sample under poling treatment, followed by PVDF-TrFE under annealing poling and PVDF under annealing. The largest sensitivity in 70/30 (no treatment) and 80/20 (poling) was only 50.0% and 46.4% of that for PVDF-TrFE. The two lowest Se among all samples occurred in 70/30 and 80/20 under annealing poling heating. In Figure 3.13, there was an increasing trend of Se for PVDF, PVDF-TrFE and 90/10 after applying these treatments. This trend might be due to the high chain mobility and low energy barrier for aligning the dipole moment in the single-phase structures and at low PVDF-TrFE weigh ratio. In contrast, Se of 70/30 and 80/20 (except poling) plateaued after applying the treatments. This plateau revealed that the dipole moment and crystalline in the materials was hardly oriented by the treatments. This might result from the low chain mobility and high energy barrier for aligning the dipole at these two weight ratios. If the PVDF-TrFE fraction rises to 50wt.%, this low degree of orientation might reverse due to the dominant self-polarized β-phase at this weight ratio.
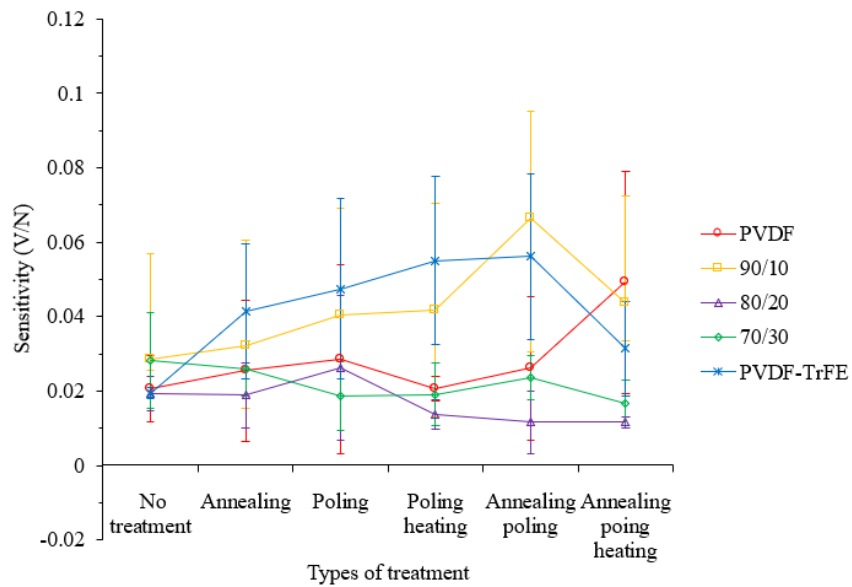
Figure 3.13. Sensitivity (Se) for samples of different weight ratios and treatments.

Table 3.8. The initial (θ_1) and rebound (θ_2) angles as well as F_{ave} for representative samples with different weight ratios.

Weight ratio	θ_1 (°)	θ_2 (°)	F_{ave} (N)
PVDF	50.46	16.51	37.91
90/10	50.41	16.30	37.70
80/20	50.43	17.17	39.12
70/30	50.37	18.16	42.54
PVDF-TrFE	50.67	18.49	44.73
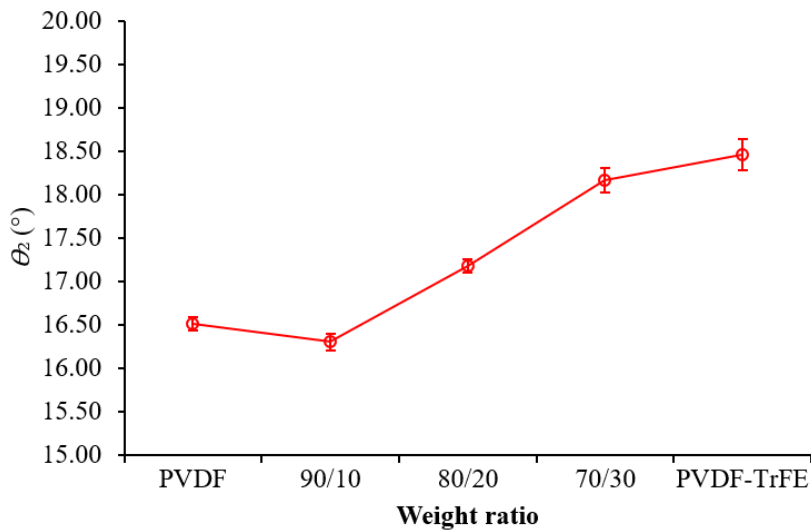
Figure 3.14. θ_2 of all samples with different weight ratios. Statistics (average and STD) were calculated based on representative samples that underwent different treatments.

Table 3.9. The largest and smallest Se for the samples at specific weight ratios, and the corresponding treatments.

Weight ratios	Largest Se (V/N)	Smallest Se (V/N)
PVDF	0.049 Annealing	0.021 Poling heating
90/10	**0.067 Annealing poling**	0.028 No treatment
80/20	0.026 Poling	0.012 Annealing poling heating
70/30	0.028 No treatment	0.017 Annealing poling heating
PVDF-TrFE	0.056 Annealing poling	0.019 No treatment

3.3. FT-IR

3.3.1. Peak identification

Representative FT-IR spectra for sample that underwent no treatment, annealing and poling heating are shown in Figure 3.15 to Figure 3.17, while the graphs for poling, annealing heating and annealing heating poling are shown in Figure A1 to Figure A3. The formation of a peak at 763 cm^{-1} was thought to result from the in-plane bending vibration (wagging) of CF$_2$ groups [40] or the rocking in the PVDF polymer chain [58], which was generally acknowledged to be the α-phase [12] [59] [60] [61]. The existence of a peak at 840 cm^{-1} was usually regarded as the rocking in CH$_2$ [40] [58], assigned to the β-phase [3] [40], or the out-of-plane combination [58] of β- and γ-phases [27] [35] [48]. The peak at 1232 cm^{-1} was assigned to the γ-phase [3] [62] but some argued it might include β-phase as well [48], which was attributed to the wagging and rocking of CH$_2$ [40] [63]. The peak at 1275 cm^{-1} was assigned exclusively to the β-phase [3] [64], resulting from the asymmetric stretching of CF$_2$ [64]. The peak at 1275 cm^{-1} could shift to a slightly larger wavenumber in pure PVDF-TrFE due to minor structural or vibrational changes of the β-phase [65]. Although peaks at other wavenumbers were mentioned in the literature such as 510 cm^{-1} and 614 cm^{-1} representing β-phase and α-phase [3] [34] respectively, these wavenumbers were either controversial [48] or not applicable for further phase content calculation.

As shown in Figure 3.15 (no treatment), for all the five weight ratios, the peak at 763 cm^{-1} was hardly noticeable, indicating that the corresponding α-phase was not dominant in the polymer chain. The weight ratio of 80/20 showed a slightly more obvious peak at 763 cm^{-1}, which represented a higher α-phase absorbance. In contrast, the peaks at 838 cm^{-1} were significant, which could be assigned to the combination of β- and γ-phases. The peaks at 1232 cm^{-1} and corresponding γ-phase were clear in PVDF and the blended polymers. However, the PVDF-TrFE curve exhibited a flatter shoulder at 1232 cm^{-1}, indicating a lower γ-phase content. At 1275 cm^{-1}, as the PVDF-TrFE weight fraction increased, a peak became more identifiable, suggesting higher β-phase content. From PVDF to 70/30 and PVDF-TrFE, the FT-IR curve witnessed a gradual transition from a pronounced γ-peak (1232 cm^{-1}) to a pronounced β-peak (1275 cm^{-1}), until the γ-peak was surpassed by the β-peak in PVDF-TrFE. By comparing Figure 3.15, Figure 3.16, Figure 3.17 and the other FT-IR graphs in Figure A1 to Figure A3, the different treatments imposed insignificant impact on phase identification.

45
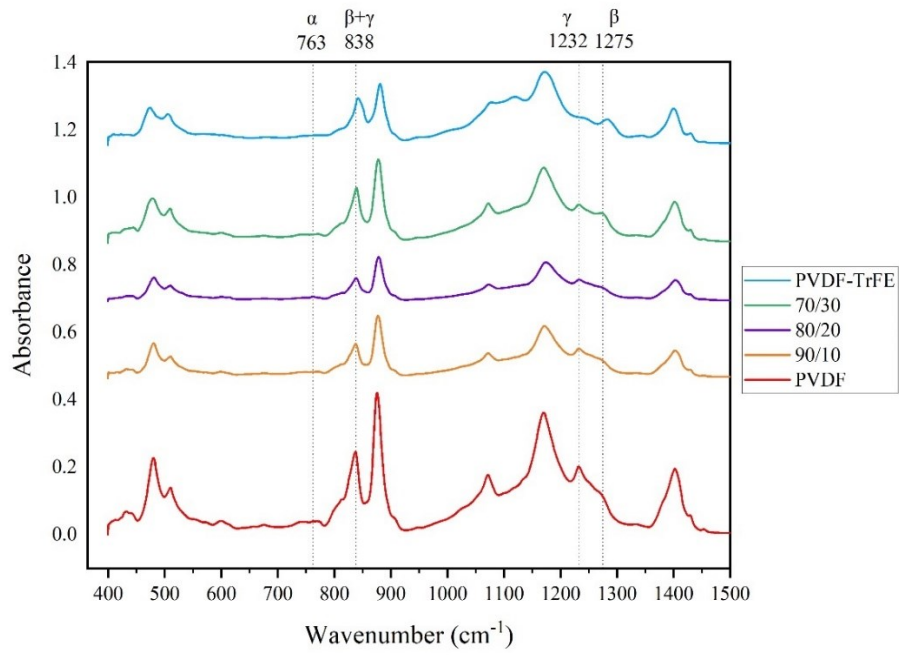
Figure 3.15. FT-IR graphs of samples with different weight ratios under no treatment.
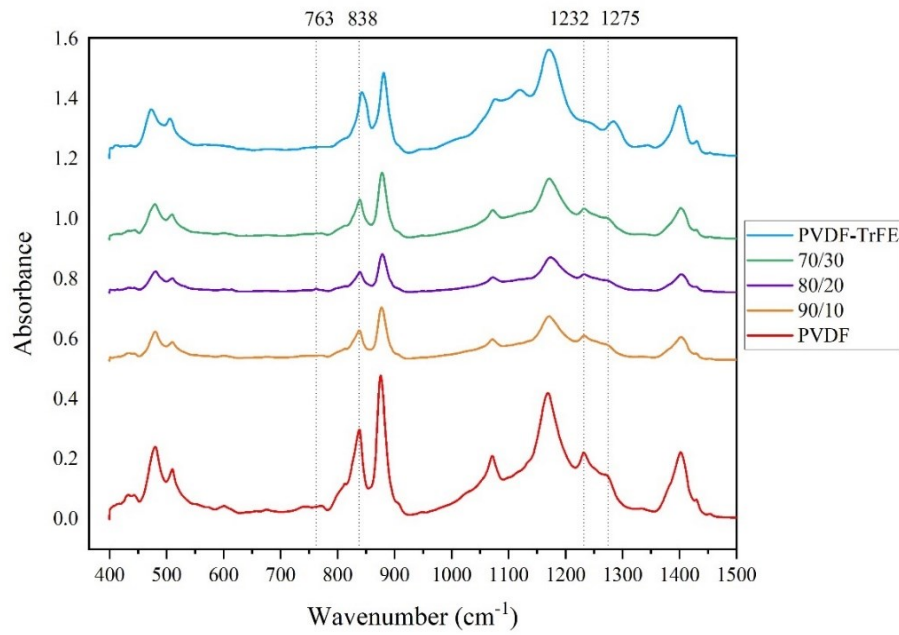
Figure 3.16. FT-IR graphs of samples with different weight ratios under annealing.
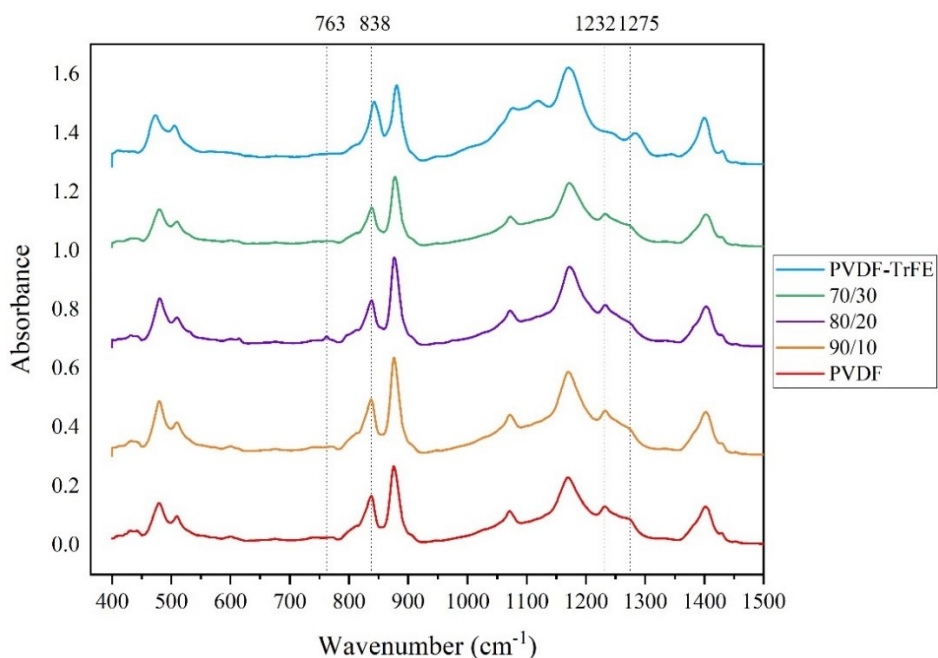
Figure 3.17. FT-IR graphs of samples with different weight ratios under poling heating.

The FT-IR spectra for representative PVDF samples subjected to different treatments are shown in Figure 3.18. Corresponding results for 80/20 and PVDF-TrFE are given in Figure 3.19 and Figure 3.20, respectively, while those for 90/10 and 70/30 are provided in Figure A4 and Figure A5. These figures confirmed that the locations of the peaks did not vary from curve to curve in the same figure, indicating that the formation of the α-, β-, and γ-phases was not significantly affected by the thermal and electrical treatments, regardless of the PVDF-TrFE fraction. As shown in Figure 3.19, every 80/20 sample showed a significant peak of absorbance at 763 cm^{-1}, indicating that this high α-phase content was independent of the type of treatment. Moreover, comparison between the FT-IR spectra in Figure 3.18 (PVDF) and in Figure 3.20 (PVDF-TrFE) confirmed a peak shift from 1275 to 1283 cm^{-1}, which corresponded to the growth of the electroactive β-phase structure after introducing the TrFE monomer into PVDF polymer chain [65].
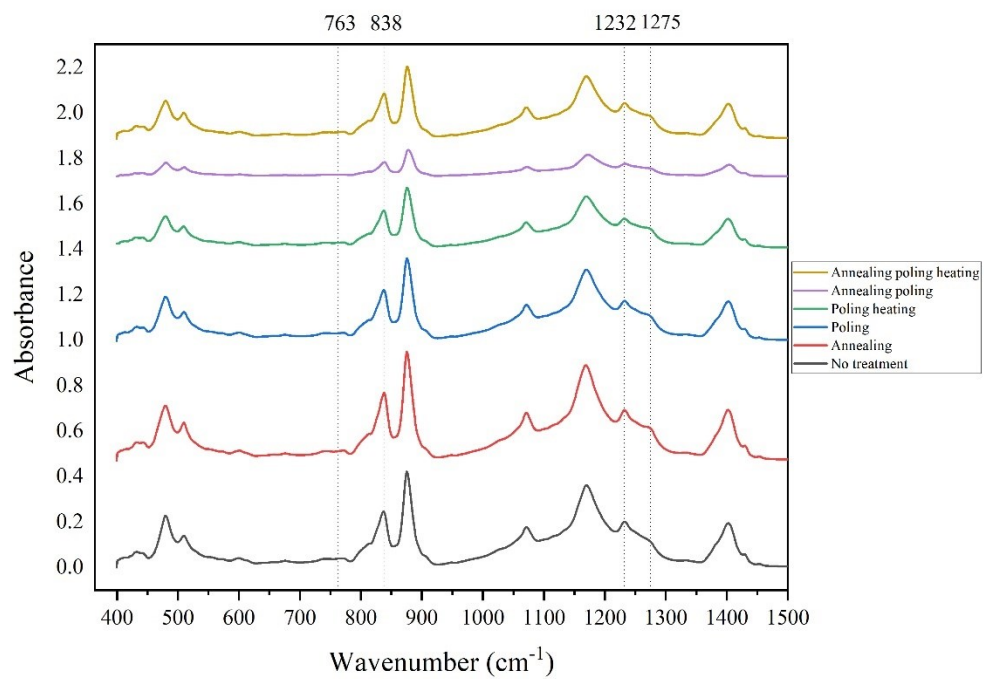
Figure 3.18. FT-IR graphs of PVDF samples under different treatments.
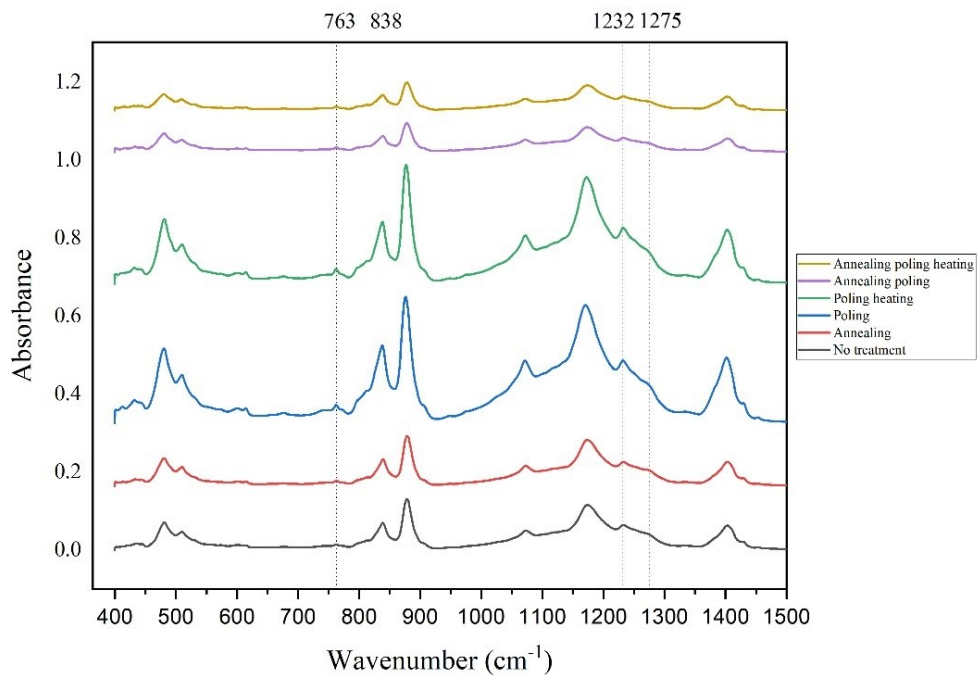
Figure 3.19. FT-IR graphs of 80/20 samples under different treatments.
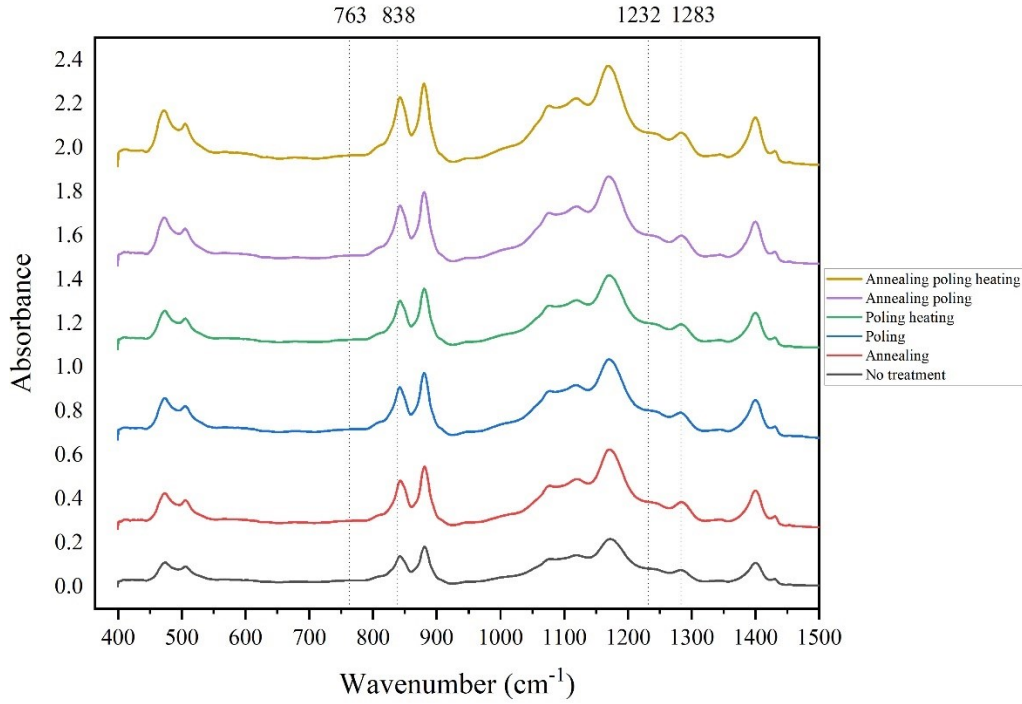
Figure 3.20. FT-IR graphs of PVDF-TrFE samples under different treatments.

3.3.2. Quantification of the α-, β- and γ- phases

Different methods have been used to analyze FT-IR graphs to not only identify but also quantify the content of specific crystalline structures, especially the polar β-phase. The feasibility of each method as applied to the samples studied in this work is discussed in this section.

The most popular way to calculate the β-phase content is the Lambert-Beer Law based on Eqn. (3.2) [3] [27], where the factor of 1.26 is obtained from the ratio between K_a and K_b, which are the absorbance coefficients at 763 cm^{-1} and 840 cm^{-1}, equal to $6.1*10^4$ and $7.7*10^4$ cm^2 mol^{-1} respectively. A_α and A_β in Eqn. (3.2) denote the absorbance at 763 and 840 cm^{-1}.

$$F(\beta) = \frac{A_\beta}{1.26A_\alpha + A_\beta} \qquad (3.2)$$

However, many argued that the β-phase percentage calculated this way contained both β- and γ-phases, because 840 cm^{-1} could also be assigned to the γ-phase [8]. Therefore $F(\beta)$ in Eqn. (3.2) evolved to the $F(\beta+\gamma)$ in Eqn. (3.3).

49

$$F(\beta + \gamma) = \frac{A_\beta}{1.26A_\alpha + A_\beta} \qquad (3.3)$$

After knowing F ($\beta+\gamma$), in order to separate F (β) and F (γ), one idea is to calculate the ratio (R_β) between F (β) and F ($\beta+\gamma$) based on the spectrum at 1275 (β) and 1232 (γ) cm^{-1}. Peaks at these two wavenumbers are thought to exclusively contain the β- and γ-phases respectively [48]. In Eqn. (3.4), R_β can be calculated using different methods, including peak height ratio (PHR) [3] [27] [35], peak height difference ratio (PHDR) and peak area ratio (PAR) [42]. Specifically, H_β and H_γ each corresponds to the absorbance of the peak in PHR (Figure 3.21), the height difference between the peak and its nearest valley in PHDR (Figure 3.26), and the area under the peak in PAR (Figure 3.27), evaluated near the wavenumbers of 1275 (β) and 1232 (γ) cm^{-1} respectively. Because the β-phase peak shifted to a higher wavenumber in PVDF-TrFE, the corresponding H_β was calculated for the peak at 1283 cm^{-1}.

$$R_\beta = \frac{H_\beta}{H_\beta + H_\gamma} \qquad (3.4)$$

After substituting R_β into Eqn. (3.5), the β-phase content can be distinguished. The fractions of α- and γ-phases are subsequently calculated using Eqn. (3.6) and Eqn. (3.7).

$$F(\beta) = F(\beta + \gamma) \times R_\beta \qquad (3.5)$$

$$F(\alpha) = 1 - F(\beta + \gamma) \qquad (3.6)$$

$$F(\gamma) = F(\beta + \gamma) - F(\beta) \qquad (3.7)$$

3.3.2.1. Peak height ratio (PHR)

This method is based on the PHR between the FT-IR absorbances at the corresponding wavenumbers. An example for PVDF is shown in Figure 3.21 (a). The sum of β- and γ- phase

content was calculated at first, followed by the individual fraction of α-, β- and γ-phases. In Figure 3.21 (b), different from PVDF and blended PVDF/PVDF-TrFE, H_β for PVDF-TrFE was evaluated at the shifted peak (1283 cm^{-1}). The α-, β-, and γ-phase contents are shown in Figure 3.22 to Figure 3.24. As seen from Table 3.10 and Figure 3.22, the α-phase of 80/20 was at the highest level, peaking at 26.84% for the sample with annealing poling. The second highest α-phase level appeared in pure PVDF-TrFE, closely followed by 90/10. The lowest α-phase content (15.03%) was found in PVDF under annealing, while the α-phase level of 70/30 was the second lowest.

As shown in Table 3.11 and Figure 3.23, the β-phase content for PVDF-TrFE was at the highest level, starting from 37.95% (no treatment) and peaking at 41.70% (annealing poling heating). Below PVDF-TrFE was 70/30, PVDF and 90/10, with 80/20 presenting the lowest β-phase content, ranging from 27.77% (poling heating) to 31.71% (annealing). According to Figure 3.23, treatment like annealing, poling and heating could improve the β-phase content in pure PVDF and PVDF-TrFE. The 90/10 sample also witnessed a slight increase in β-phase content after annealing. Contrarily, for the blended polymers of 80/20 and 70/30, the treatments seemed not improve their β-phase content. As mentioned in Section 3.2.3, as the PVDF-TrFE content in two-phase PVDF/PVDF-TrFE increased from 10 to 30wt.%, the energy barrier for orienting the blended polymer chains was elevated. Therefore, the transformation from α- to β-phase by treatments became more difficult compared to single-phase PVDF and PVDF-TrFE as well as the blend at low PVDF-TrFE weight ratio (90/10).

In Table 3.12 and Figure 3.24, PVDF showed the highest level of γ-phase content, peaking at 53.28% (no treatment), while pure PVDF-TrFE samples exhibited the lowest γ-phase content, with the smallest value at around 40.80% (poling heating). As summarized in Figure 3.25, according to the PHR method and regardless of the treatment, the γ-phase was dominant in pure PVDF and the three blended polymers. Conversely, the contents of β- and γ-phases in PVDF-TrFE were comparable to each other. The higher β-phase content in PVDF-TrFE could explain the high voltage output in the pendulum impact test, while the lowest electrical output for 80/20 samples was consistent with its low β-phase fraction. Generally, as the PVDF-TrFE weight fraction increased, the γ-phase content tended to decrease, except a slight increase in γ-phase content of the 70/30 sample when compared to 80/20.

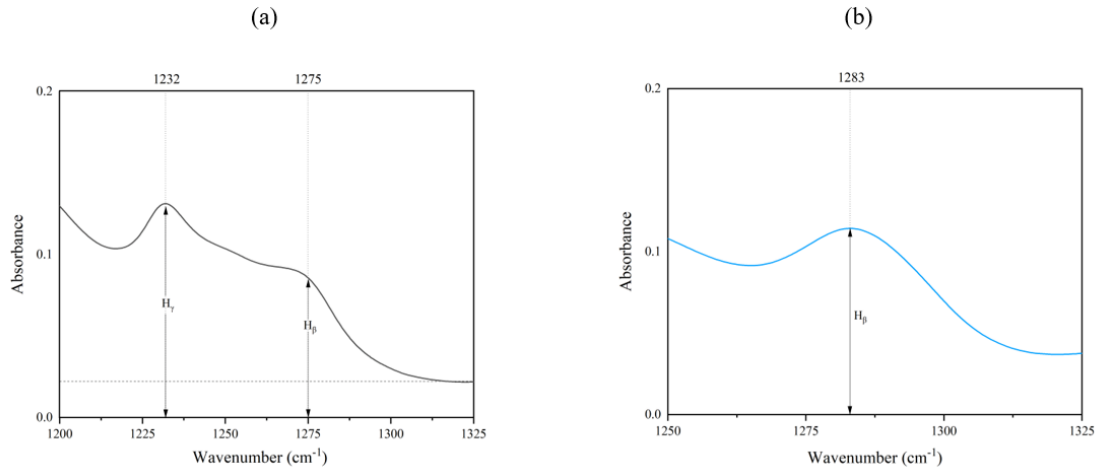Figure 3.21. PHR calculation example for (a) PVDF and blended PVDF/PVDF-TrFE (b) PVDF-TrFE.
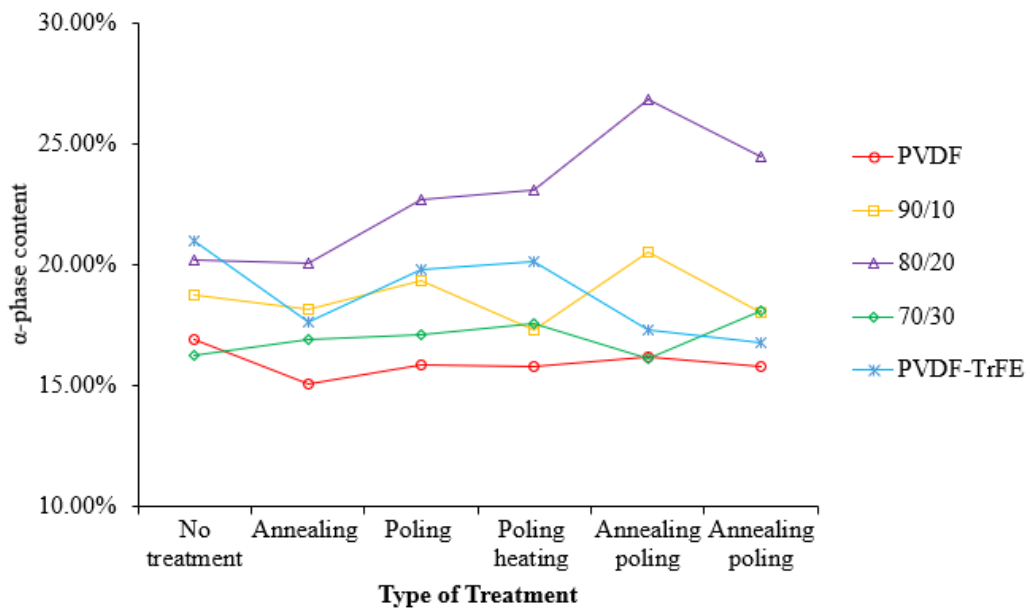
Figure 3.22. α-phase content for samples with different weight ratios and treatment, calculation based on PHR.
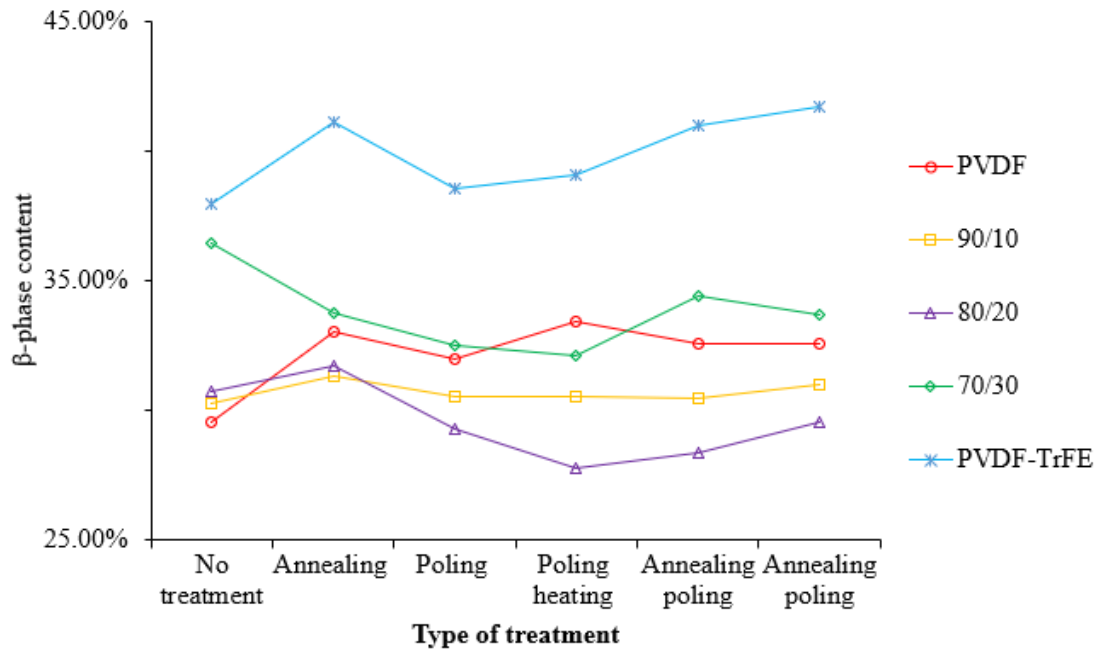
Figure 3.23. β-phase content for samples with different weight ratios and treatment, calculation based on PHR.
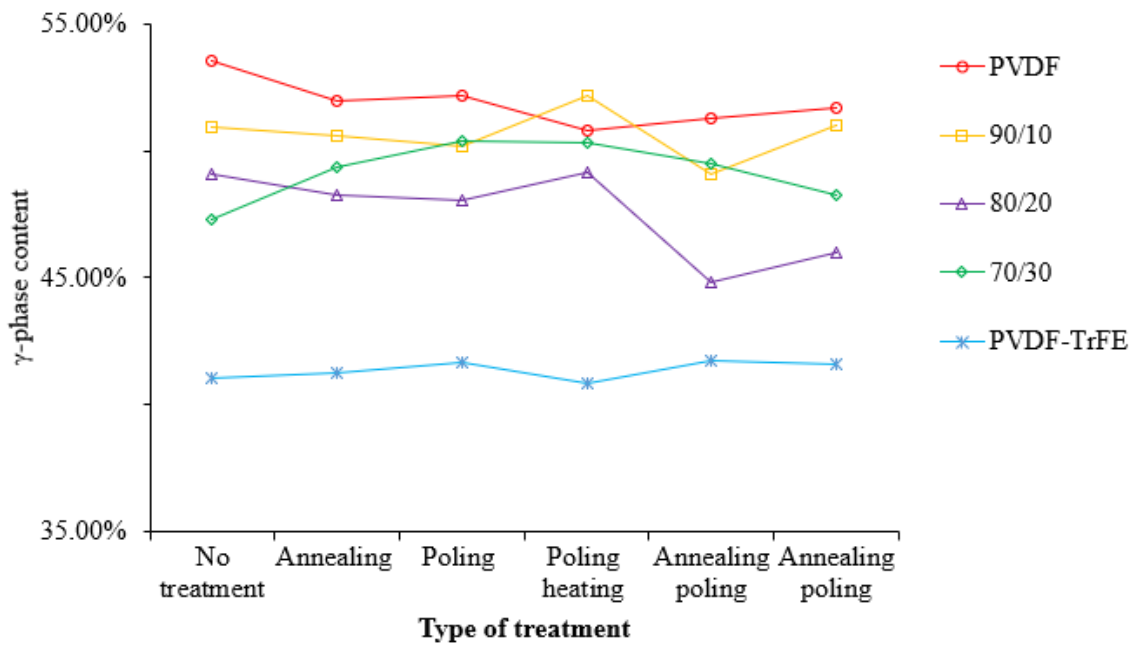
Figure 3.24. γ-phase content for samples with different weight ratios and treatment, calculation based on PHR.

Table 3.10. The maximum, minimum and average α-phase contents of samples at specific weight ratios and the corresponding treatments. Average was performed over samples that underwent different treatments.

Weight ratios	Maximum α	Minimum α	Average α
PVDF	16.93% No treatment	15.03% Annealing	15.92%
90/10	20.49% Annealing poling	17.31% Poling heating	18.68%
80/20	26.84% Annealing poling	20.06% Annealing	**_22.89%_**
70/30	18.08% Annealing poling heating	16.16% Annealing poling	17.00%
PVDF-TrFE	21.00% No treatment	17.31% Annealing poling	18.76%

Table 3.11. The maximum, minimum and average β-phase contents of samples at specific weight ratios and the corresponding treatments. Average was performed over samples that underwent different treatments.

Weight ratios	Maximum β	Minimum β	Average
PVDF	33.39% Poling heating	29.50% No treatment	32.16%
90/10	31.28% Annealing	30.28% No treatment	30.66%
80/20	31.71% Annealing	27.77% Poling heating	29.55%
70/30	36.43% No treatment	32.13% Poling heating	33.81%
PVDF-TrFE	41.70% Annealing poling heating	37.95% No treatment	**_39.90%_**

Table 3.12. The maximum, minimum and average γ-phase contents of samples at specific weight ratios and the corresponding treatments. Average was performed over samples that underwent different treatments.

Weight ratios	Maximum γ	Minimum γ	Average
PVDF	53.58% No treatment	50.84% Poling heating	**51.92%**
90/10	52.19% Poling heating	49.09% Annealing poling	50.66%
80/20	49.15% Poling heating	44.80% Annealing poling	47.55%
70/30	50.39% Poling	47.33% No treatment	49.19%
PVDF-TrFE	41.71% Annealing poling	40.80% Poling heating	41.34%

Figure 3.25. α-, β- and γ-phase contents for samples with different weight ratios, calculation based on PHR. Statistics (average and STD) were calculated based on samples that underwent different treatments.
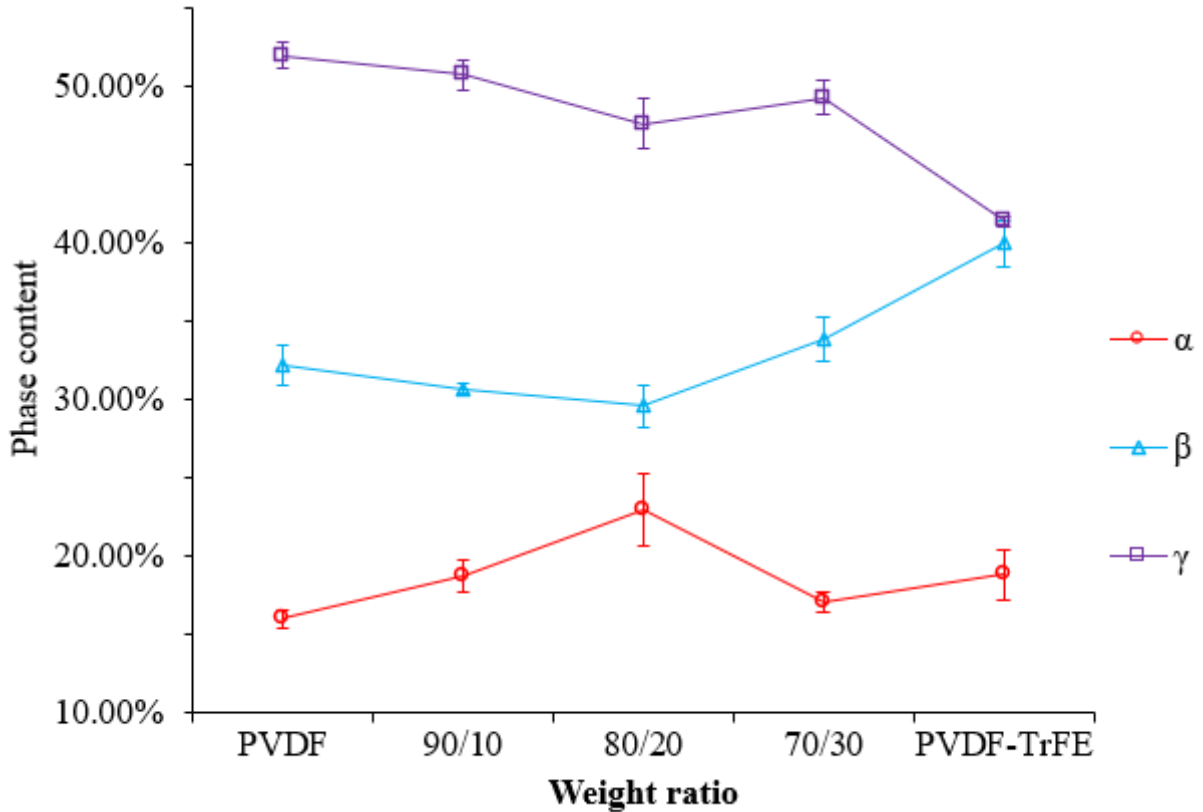
3.3.2.2. Peak height difference ratio (PHDR)

As shown in Figure 3.26 (a) for the PVDF sample, H_γ in Eqn. (3.4) was calculated as the difference between the absorbance at the peak of 1232 cm^{-1} and its nearest valley at 1217 cm^{-1}. H_β was calculated as the difference between the absorbance at the peak of 1275 cm^{-1} and its nearest valley at around 1325 cm^{-1}. For PVDF-TrFE, H_γ was calculated as the difference between the absorbance at the peak of 1232 cm^{-1} (γ-phase) and its nearest valley at 1265 cm^{-1}. However, when calculating H_β, there was ambiguity regarding the nearest valley to the peak at 1283 cm^{-1} (β-phase). In Figure 3.26 (b), if the valley was chosen on the left-hand side (LHS) of 1283 cm^{-1}, at 1265 cm^{-1}, the calculated β-phase content was 31.74%. If the valley was chosen on the right-hand side (RHS) of 1283 cm^{-1}, at 1325 cm^{-1}, the calculated β-phase content was 57.06%.

The β-phase contents for non-treated samples were calculated as an example and listed in Table 3.13. The PVDF sample showed 54.23% β-phase content. In comparison, 31.74% was an irrationally low value for PVDF-TrFE. Even if 57.06% was chosen as the β-phase content for PVDF-TrFE, it was till lower than the result for the 70/30 (67.61%) and 80/20 (58.41%) samples. This was unphysical and inconsistent with the earlier results from the pendulum impact test in section 3.2. Therefore, the method of PHDR was not applied in the final β-phase content calculation.
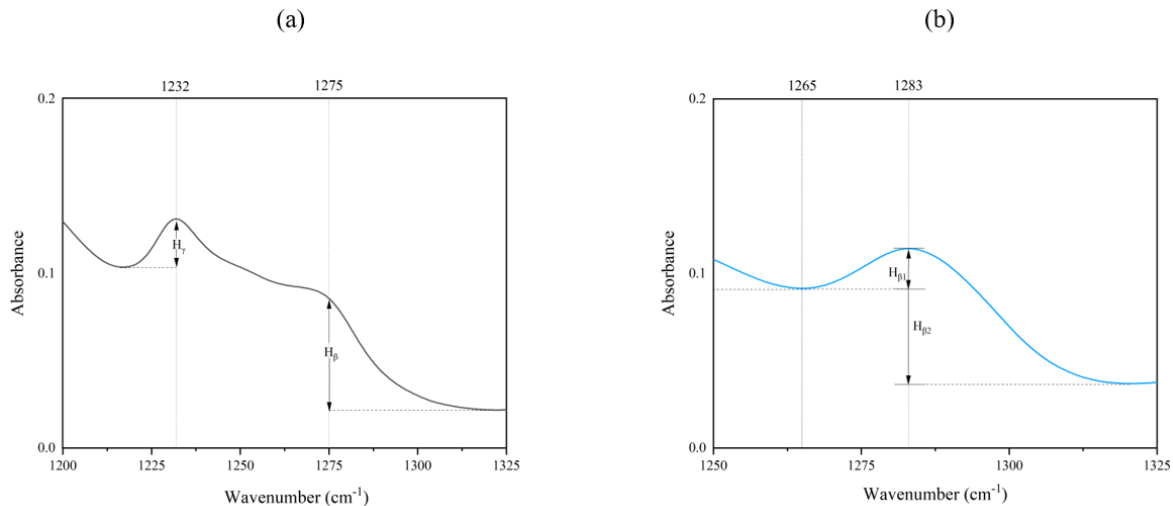
(a) (b)

Figure 3.26. PHDR calculation example of (a) PVDF and PVDF/PVDF-TrFE (b) PVDF-TrFE.

Table 3.13. Trial calculation of β-content from PHDR.

Treatment	Weight ratio	β phase content
	PVDF	54.23%
	90/10	54.87%
No treatment	80/20	58.41%
	70/30	67.61%
	PVDF-TrFE	57.06%

3.3.2.3. Peak area ratio (PAR)

The peak area in PAR is calculated as the area under the FT-IR curve between the peaks and baselines of interest. According to Cai et al., β-phase content calculated by PHR was equivalent to that from PAR, which was determined by the OMNIC software from Thermo Scientific. The selection of baselines and integration methods was automatically determined by this software [48]. In order to investigate the how the PAR was applied and to extract additional information in comparison to PHR, the baselines were manually selected, depending on the shape of the targeted peaks. In Figure 3.27 (a), the baseline for H_γ was tangent to the nearest valley on the LHS of the peak at 1232 cm^{-1}. The baseline for H_β was tangent to the nearest valley on the RHS of the peak at 1275 cm^{-1}. The same principle was applied to calculate PAR for PVDF-TrFE in Figure 3.27 (b), while the β- and γ-peaks shifted to higher wavenumbers. Figure 3.28 shows the β-phase content for samples with different weight ratios and treatment, calculated based on PAR. PVDF-TrFE exhibited exceptionally higher β-phase level than the other weight ratios. 70/30 showed the second highest β-phase level, followed by PVDF and 80/20, while 90/10 showed the lowest β-phase content. This cannot explain the much lower output voltage and sensitivity (*Se*) of 80/20 compared to 90/10 showed in section 3.2.2 and 3.2.3. When compared, the results from PAR and PHR (section 3.3.2.1) were not entirely consistent. Both methods did, however, predict the higher β-phase content in PVDF-TrFE, consistent with its excellent piezoelectric response.
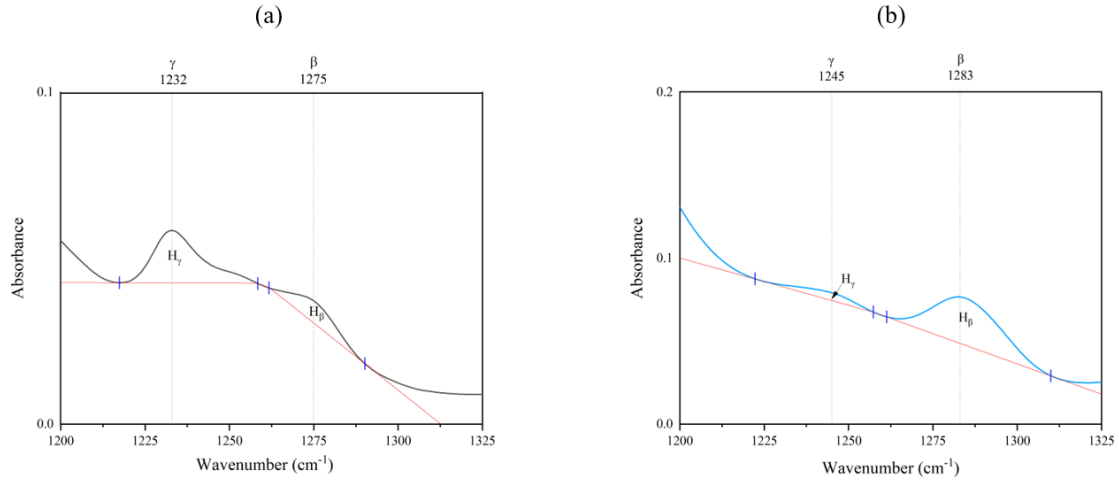
Figure 3.27. PAR calculation example of (a) PVDF and PVDF/PVDF-TrFE (b) PVDF-TrFE.
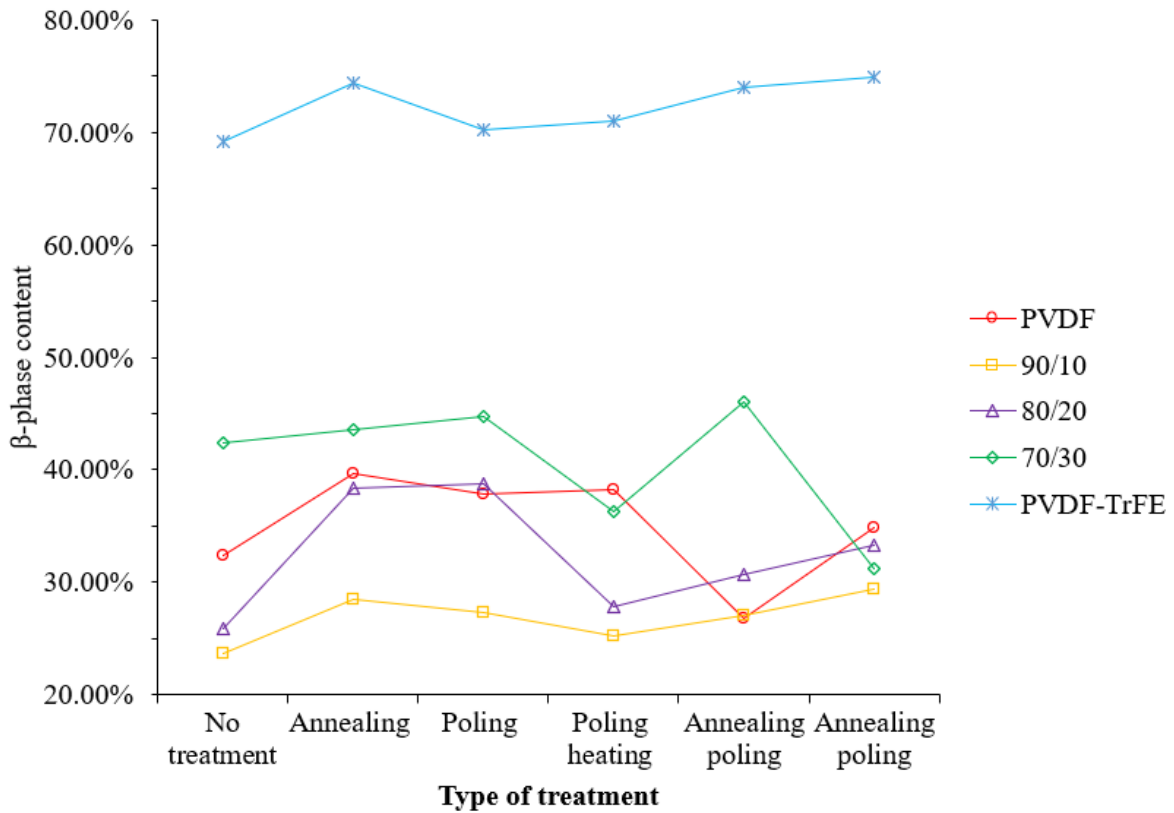

Figure 3.28. β-phase content for samples with different weight ratios and treatment, calculation based on PAR.

3.3.2.4. Integrated area ratio (IAR)

Different from PAR, IAR is a method where multiple peaks are selected with a specific

range. The integrated areas under the peaks are calculated with a single baseline by functions such as Lorentz, Gaussian, Voight etc. An example adapted from Cai et al. to calculate IAR of PVDF is shown in Figure 3.29 (a). Within the range from 780 to 920 cm^{-1}, the peak at 838 cm^{-1} was assumed to represent the combination of β-phase and γ-phase. Several integrated areas were generated under these peaks. Among them, $H_β$ and $H_γ$ at 838 cm^{-1} was assumed to represent β-phase and γ-phase respectively. According to Eqn. (3.4) and Eqn. (3.5), the $R_β$ was then calculated as well as the β-phase content. However, how these two integrated areas were generated at 838 cm^{-1} and corresponding to β-phase and γ-phase were not well explained in the work of Cai et al [48]. An attempt to reproduce their work is shown in Figure 3.29 (b). According to the location of those integrated areas in Figure 3.29 (a), three dominant peaks were automatically identified by the Origin software at 812, 838 and 876 cm^{-1}. Except for 838 cm^{-1}, the other two wavenumbers did not seem to represent specific crystalline phases, and only had numerical meanings. These peaks were then manually selected for the settings of multiple peak fit in Origin. Lorentz function was used to calculate the integrated areas, with the defaulted baseline along x-axis. As shown in Figure 3.29 (b), two integrated areas of (H_1) and (H_2) are located at 838m^{-1}. According to Origin computation, the smaller H_1 was called fit peak, corresponding to the peak that was manually selected in the last step. The larger H_2 was denoted as cumulative peak fit, representing the sum of all potential peaks (significant or insignificant) at this wavenumber. Overall, the approach of using the two integrated peak areas at 838m^{-1} to distinguish the β-phase and γ-phase was not deemed appropriate, since the ratio between them had no clear correspondence to the crystalline structures. Therefore, IAR method was not utilized in the final β-phase content analysis.
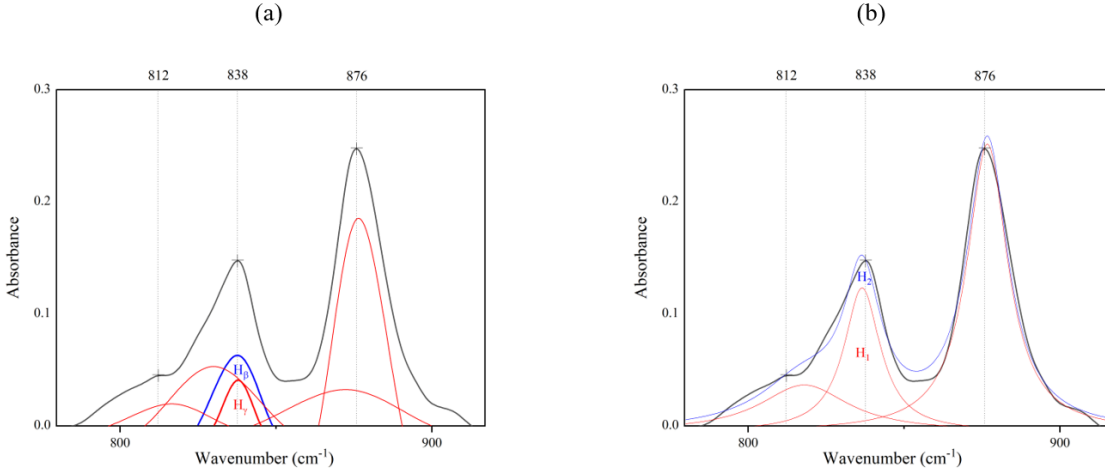
Figure 3.29. IAR calculation example of PVDF from (a) Cai et al. [48] (b) our work.

3.3.2.5. PHR based on one literature

According to Zhang et al., β-phase content of PVDF and blended PVDF-TrFE could be calculated by using Eqn. (3.8), where A represented the absorbance values for 614, 510 and 1275 cm^{-1} which corresponded to α, β and γ phases respectively. Additionally, the peak that corresponded to the β-phase for PVDF-TrFE shifted to a higher wavenumber of 1283 cm^{-1} [34].

$$F(\beta) = \frac{A_{510}}{A_{614(\alpha)} + A_{510(\beta)} + A_{1275(\gamma)}} \qquad (3.8)$$

Figure 3.30 shows the FT-IR spectra for non-treated PVDF, where the peaks are classified according to Zhang et al. The most controversial part of this method was that the peak at 1275 cm^{-1} was identified as γ- phase instead of β- phase. As the PVDF-TrFE fraction increased, the peak at 1275 cm^{-1} was elevated, which would indicate a higher γ- phase level. Results calculated by this special PAR method for non-treated samples are shown in Table 3.14. The β-phase content of PVDF-TrFE was the lowest within the five weight ratios, which was unphysical and inconsistent with the pendulum impact results in section 3.2. Therefore, this method was not applied in the final analysis.
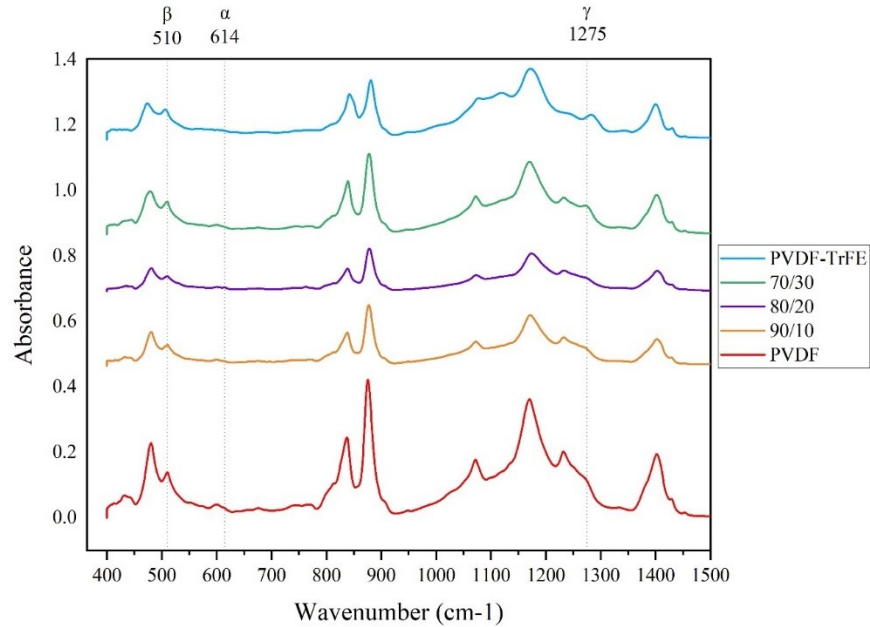
Figure 3.30 FT-IR graphs of samples with different weight ratios under no treatment, with the wavenumbers classified according to Zhang et al. [34].

Table 3.14. Trial calculation of β-content based on the method of Zhang et al. [34].

Treatment	Weight ratio	β phase content
No treatment	PVDF	39.57%
	90/10	39.65%
	80/20	40.36%
	70/30	41.35%
	PVDF-TrFE	38.90%

To summarize the FT-IR analysis, after comparing and contrasting the aforementioned five methods in practice, the result based on PHR method was physical and consistent with the earlier results from the pendulum impact test in Section 3.2. Besides, the results from PAR and PHR both predict the higher β-phase fraction in PVDF-TrFE, consistent with its superior piezoelectric response.

Chapter 4. Conclusion and Future Work

4.1. Conclusion

PVDF-TrFE as a highly electroactive but expensive copolymer of PVDF shows excellent ferroelectric and piezoelectric properties. In this research, blending PVDF-TrFE with its homopolymer was feasible to enhance the piezoelectric behavior while remaining a reasonable cost. Extruded filaments and spin-coated thin films of blended PVDF and PVDF-TrFE were successfully manufactured. The impact sensor based on spin-coated PVDF/PVDF-TrFE was fabricated, while a pendulum impact test apparatus was designed to quantify the mechanical potential, and the responded kinetic energy and electrical output could be calculated and measured respectively. The effect of blending weight ratios, thermal and electrical treatment on the mechanical and electromechanical properties was investigated. FT-IR characterization was carried out to explain the correlation between the electroactive β-phase content and voltage results in the pendulum impact test. The key findings are summarized as below.

- **Effect on Mechanical Properties**

As the PVDF-TrFE weight fraction increased from 0 to 30wt.%, the elastic modulus and ultimate tensile strength of the PVDF/PVDF-TrFE filament decreased. Nonetheless, this decline in mechanical properties roughly follow the rule of mixture, in spite of some fluctuations. Moreover, the annealing treatment on the filament brought a decrease in both elastic modulus and ultimate tensile strength. This decline in mechanical properties might be caused by the microstructure defects formation, overshadowing the potential enhancement related to improved crystallinity and orientation.

- **Effect on Electrical Output and Sensitivity of Impact Sensor**

Four different voltage patterns were observed during the impact test, including (+;-), (-;+), (+) and (-) modes. During the first impact, the initial maximum positive or negative voltage was regarded as the piezoelectric output. The different sign of the first peak might result from multiple reasons including the variation of the sample fabrication and inherent material features. Nonetheless, the different sign of output voltage did not affect the magnitude analysis. For V_{pm} of the samples, the pure PVDF-TrFE presented the highest level, followed by 90/10, while 80/20 and 70/30 presented a much lower V_{pm}. For the V_{nm}, PVDF-TrFE still exhibited the highest level, followed by 90/10, 70/30, 80/20 and PVDF. The largest V_{nm} was found in a 90/10 sample under

annealing poling. The thermal and electrical treatment tended to be effective for generating a higher output, especially in the pure polymer components and 90/10. For the electrochemical sensitivity calculated from peak-to-peak voltage, the ranking of the Se level was similar to one in $V_{\text{pk-pk}}$. The single-phase PVDF-TrFE had the highest level due to its excellent k_{33}, followed by 90/10. However, PVDF became more sensitive than 70/30 and 80/20. As the PVDF-TrFE weight ratios exceeded 20wt.%, the low chain mobility and presence of interface might inhibit the polymer chain mobility and conversion between mechanical and electrical energy in the two-phase immiscible polymer blends.

- **Effect on FT-IR Spectra Characterization**

By using the commination of Lambert-Beer Law and PHR method to quantify FT-IR spectra results. The 80/20 exhibited the lowest average β-phase content, resulting from the highest α-phase in this weight ratio. Meanwhile, the α-phase of all weight ratios remained at a low level. The γ-phase was found to be the most dominant in all weight ratios. As the PVDF weight ratio increased, the γ-phase content generally became higher, though there was a sudden increasement in γ-phase content of 70/30 in comparison to the one of 80/20. The β- and γ-phase level in PVDF-TrFE were close to each other. Specifically, it was found that PVDF-TrFE under annealing poling heating obtained the highest maximum β-phase content, followed by the group of 70/30 no treatment, PVDF poling heating, 80/20 annealing, and 90/10 annealing. Besides, the PAR method showed exceptionally high β-phase content in PVDF-TrFE.

To summarize, the decent electrical output for PVDF-TrFE impact sensor were related to its high β-phase content, while the poor performance for 80/20 samples had inseparable relationship with its low β-phase level. Also, the abundant β-phase content in 70/30, 90/10 and PVDF maintained the electrical output at a good level.

4.2. Future work

Based on the current study, further effort involving more systematic parameter optimization on manufacture, thermal and electrical treatment is expected to improve the mechanical and electrical performance of the blended PVDF/PVDF-TrFE. Various characterizations can be applied on this polymer blend to better explain the crystalline structure change and phase transformation after changing PVDF-TrFE weight fraction and under different treatment methods.

PVDF/PVDF-TrFE can also be produced through diverse manufacture methods and be utilized in versatile applications.

- **Parameter and apparatus optimization**

Apart from the three blended PVDF/PVDF-TrFE weight ratios studied in the current research, more combinations such as 60/40, 50/50, 40/60, 30/70, 20/80, and 10/90 can be investigated in extrusion and spin-coating method. Therefore, the effect of the dominant PVDF-TrFE weight fraction in this polymer blend can be better understood, while the cost effectiveness in application should be also considered.

In the extrusion of PVDF/PVDF-TrFE filament, more consistent and evener diameter is expected to be controlled by introducing the air-quenching and conveyor system. Therefore, the instability during the mechanical test can be minimized.

For the annealing process, more systematic investigation on the effect of annealing temperature and annealing time on the crystalline structure, mechanical and electrical performance of the polymer blend can be attempted. For the electrical poling process, the experiment on the effect of poling temperature, poling time and heating temperature on the crystalline structure, electrical and mechanical performance can be carried out in a comprehensive way. Besides, A more standardized impact test setup can be redesigned to increase the impact test stability and repeatability. For example, a pinned solid beam/rod may replace the plastic string connected to the steel ball, in order to ensure the pendulum to move along the tangential direction and minimize the energy dissipation during the deformation in the string.

- **Characterization**

X-Ray Diffraction (XRD) can be used to assist the peak identification with FT-IR, providing more information about crystalline phase distribution. Scanning Electron Microscopy (SEM) can be used to observe polymer crystalline structure and defects such as grain size and phase separation, etc., helping understand the effect of PVDF-TrFE addition and treatment on the polymer microstructure, especially for the α-, β- and γ-phase transformation.

- **Melt-electrospinning and electrospinning**

By introducing the in-situ electrical poling system to our mini-extruder, the melt-electrospinning (MES) of blended PVDF/PVDF-TrFE is expected to produce fibers in micrometers diameter or at even lower scale. Therefore, the dipole and crystalline in the fibers

can be more easily orientated and aligned by the electric field when the material is in the melted state, providing higher poling effectiveness and efficiency. Additionally, this non-solvent manufacturing method is eco-friendlier and more sustainable. Secondly, electrospinning is capable of fabricating fibers in nano-scale diameter, while the toxic solvent should be paid exceptionally high attention to. Higher aspect ratio of fibers may bring better mechanical performance to the produced fibers and versatility in applications. The fiber can be either fabricated as mat or yarn, which can be applied for different forms of electrical output measurement. More complex manufacture like fabric production can be further introduced to sensor, actuator, and other applications.

- **Predicting the Mechanical Properties and electrical output**

As the PVDF-TrFE weight fraction increases, the semi-crystalline structure might be furtherly altered by the dominant PVDF-TrFE. Therefore, the effect of the low elastic modulus and ultimate tensile strength of PVDF-TrFE on the blending might be difficult to predict by rule of mixture. Various models can be applied to provide more insightful understanding of the mechanical properties of the blended PVDF/PVDF-TrFE. The comparison between models for composite materials such as Series, Parallel, and rule of Reciprocal or more complicated method like Mori-Tanaka model can be carried out, and the model most suitable for PVDF/PVDF-TrFE can be determined. Besides, models to explain the correlation between the electric output and material or processing parameters can be attempted based on further modelling and analysis including machine learning etc.

Reference

[1]   D. E. Septiyani Arifin and J. J. Ruan, "Study on the curie transition of P(VDF-TrFE) copolymer," in *IOP Conference Series: Materials Science and Engineering*, Feb. 2018, vol. 299, no. 1. doi: 10.1088/1757-899X/299/1/012056.

[2]   Y. Li, C. Liao, and S. C. Tjong, "Electrospun polyvinylidene fluoride-based fibrous scaffolds with piezoelectric characteristics for bone and neural tissue engineering," *Nanomaterials*, vol. 9, no. 7. MDPI AG, Jul. 01, 2019. doi: 10.3390/nano9070952.

[3]   P. Martins, A. C. Lopes, and S. Lanceros-Mendez, "Electroactive phases of poly(vinylidene fluoride): Determination, processing and applications," *Progress in Polymer Science*, vol. 39, no. 4. Elsevier Ltd, pp. 683–706, 2014. doi: 10.1016/j.progpolymsci.2013.07.006.

[4]   C. Ribeiro *et al.*, "Electroactive poly(vinylidene fluoride)-based structures for advanced applications," *Nature Protocols*, vol. 13, no. 4, pp. 681–704, Apr. 2018, doi: 10.1038/nprot.2017.157.

[5]   S. Sukumaran, S. Chatbouri, D. Rouxel, E. Tisserand, F. Thiebaud, and T. ben Zineb, "Recent advances in flexible PVDF based piezoelectric polymer devices for energy harvesting applications," *Journal of Intelligent Material Systems and Structures*, vol. 32, no. 7, pp. 746–780, Apr. 2021, doi: 10.1177/1045389X20966058.

[6]   S. Mishra, L. Unnikrishnan, S. K. Nayak, and S. Mohanty, "Advances in Piezoelectric Polymer Composites for Energy Harvesting Applications: A Systematic Review," *Macromolecular Materials and Engineering*, vol. 304, no. 1. Wiley-VCH Verlag, Jan. 01, 2019. doi: 10.1002/mame.201800463.

[7]   D. A. Porter, T. V. T. Hoang, and T. A. Berfield, "Effects of in-situ poling and process parameters on fused filament fabrication printed PVDF sheet mechanical and electrical properties," *Additive Manufacturing*, vol. 13, pp. 81–92, Jan. 2017, doi: 10.1016/j.addma.2016.11.005.

[8]   C. B. Lee and J. A. Tarbutton, "Polyvinylidene fluoride (PVDF) direct printing for sensors and actuators," *International Journal of Advanced Manufacturing Technology*, vol. 104, no. 5–8, pp. 3155–3162, Oct. 2019, doi: 10.1007/s00170-019-04275-z.

[9]   J.-Y. Ke, H.-J. Chu, Y.-H. Hsu, and C.-K. Lee, "A highly flexible piezoelectret-fiber pressure sensor based on highly aligned P(VDF-TrFE) electrospun fibers," in *Active and Passive Smart Structures and Integrated Systems 2017*, Apr. 2017, vol. 10164, p. 101642X. doi: 10.1117/12.2259854.

[10]   H. Kim, F. Torres, Y. Wu, D. Villagran, Y. Lin, and T.-L. Tseng, "Integrated 3D printing and corona poling process of PVDF piezoelectric films for pressure sensor application," *Smart Materials and Structures*, vol. 26, no. 8, p. 085027, Aug. 2017, doi: 10.1088/1361-665x/aa738e.

[11]   M. Marandi and J. Tarbutton, "Additive manufacturing of single- And double-layer piezoelectric PVDF-TrFE copolymer sensors," 2019, vol. 34, pp. 666–671. doi: 10.1016/j.promfg.2019.06.194.

[12]   S. Bodkhe, P. S. M. Rajesh, F. P. Gosselin, and D. Therriault, "Simultaneous 3D Printing and Poling of PVDF and Its Nanocomposites," *ACS Applied Energy Materials*, vol. 1, no. 6, pp. 2474–2482, Jun. 2018, doi: 10.1021/acsaem.7b00337.

[13]   Z. C. Kennedy *et al.*, "3D-printed poly(vinylidene fluoride)/carbon nanotube composites as a tunable, low-cost chemical vapour sensing platform," *Nanoscale*, vol. 9, no. 17, pp.

5458–5466, 2017, doi: 10.1039/c7nr00617a.

[14] J. S. Dodds, F. N. Meyers, and K. J. Loh, "Enhancing the piezoelectric performance of PVDF-TrFE thin films using zinc oxide nanoparticles," in *Sensors and Smart Structures Technologies for Civil, Mechanical, and Aerospace Systems 2012*, Apr. 2012, vol. 8345, p. 834515. doi: 10.1117/12.915072.

[15] C. Chen *et al.*, "3D printing of electroactive PVDF thin films with high β-phase content," *Smart Materials and Structures*, vol. 28, no. 6, May 2019, doi: 10.1088/1361-665X/ab15b7.

[16] W. Xia and Z. Zhang, "PVDF-based dielectric polymers and their applications in electronic materials," *IET Nanodielectrics*, vol. 1, no. 1. Institution of Engineering and Technology, pp. 17–31, 2018. doi: 10.1049/iet-nde.2018.0001.

[17] S. Men, Z. Gao, R. Wen, J. Tang, and J. M. Zhang, "Effects of annealing time on physical and mechanical properties of PVDF microporous membranes by a melt extrusion-stretching process," *Polymers for Advanced Technologies*, vol. 32, no. 6, pp. 2397–2408, Jun. 2021, doi: 10.1002/pat.5268.

[18] S. Kaur, A. Kumar, A. L. Sharma, and D. P. Singh, "Influence of annealing on dielectric and polarization behavior of PVDF thick films," *Journal of Materials Science: Materials in Electronics*, vol. 28, no. 12, pp. 8391–8396, Jun. 2017, doi: 10.1007/s10854-017-6556-8.

[19] S. Satapathy, S. Pawar, P. K. Gupta, and B. R. Varma, "Effect of annealing on phase transition in poly(vinylidene fluoride) films prepared using polar solvent," 2011.

[20] R. Buchdahl, "Mechanical properties of polymers and composites – Vols. I and II, Lawrence E. Nielsen, Marcel Dekker, Inc., New York, 1974, Vol. I pp. 255, Vol. II pp. 301," *Journal of Polymer Science: Polymer Letters Edition*, vol. 13, no. 2, pp. 120–121, Feb. 1975, doi: 10.1002/pol.1975.130130214.

[21] M. Satthiyaraju and T. Ramesh, "Effect of annealing treatment on PVDF nanofibers for mechanical energy harvesting applications," *Materials Research Express*, vol. 6, no. 10, Sep. 2019, doi: 10.1088/2053-1591/ab4037.

[22] X. Li and X. Lu, "Effect of annealing on the structure and properties of polyvinylidene fluoride hollow fiber by melt-spinning," *Journal of Applied Polymer Science*, vol. 103, no. 2, pp. 935–941, Jan. 2007, doi: 10.1002/app.25255.

[23] H. Yan, L. Yayan, and Y. Yifei, "Simultaneous stretching and static electric field poling of poly(vinylidene fluoride-hexafluoropropylene) copolymer films," in *Polymer Engineering and Science*, Oct. 2007, vol. 47, no. 10, pp. 1630–1633. doi: 10.1002/pen.20843.

[24] J. L. Lutkenhaus, K. McEnnis, A. Serghei, and T. P. Russell, "Confinement effects on crystallization and curie transitions of poly(vinylidene fluoride-co-trifluoroethylene)," *Macromolecules*, vol. 43, no. 8, pp. 3844–3850, Apr. 2010, doi: 10.1021/ma100166a.

[25] B. Neese *et al.*, "Piezoelectric responses in poly(vinylidene fluoride/hexafluoropropylene) copolymers," *Applied Physics Letters*, vol. 90, no. 24, 2007, doi: 10.1063/1.2748076.

[26] M. W. Mohamad Hafiz *et al.*, "Effect of annealing temperature on the crystallinity, morphology and ferroelectric of polyvinylidenefluoride-trifluoroethylene (PVDF-TrFE) thin film," in *Advanced Materials Research*, 2013, vol. 812, pp. 60–65. doi: 10.4028/www.scientific.net/AMR.812.60.

[27] N. Meng, X. Zhu, R. Mao, M. J. Reece, and E. Bilotti, "Nanoscale interfacial electroactivity in PVDF/PVDF-TrFE blended films with enhanced dielectric and ferroelectric properties," *Journal of Materials Chemistry C*, vol. 5, no. 13, pp. 3296–3305, 2017, doi: 10.1039/c7tc00162b.

[28] N. Meng *et al.*, "Processing and characterization of free standing highly oriented ferroelectric polymer films with remarkably low coercive field and high remnant polarization," *Polymer*, vol. 100, pp. 69–76, Sep. 2016, doi: 10.1016/j.polymer.2016.08.017.

[29] D. R. Paul, "Background and Perspective," in *Polymer Blends*, Elsevier, 1978, pp. 1–14. doi: 10.1016/B978-0-12-546801-5.50007-4.

[30] S. Krause, "Polymer–Polymer Compatibility," in *Polymer Blends*, Elsevier, 1978, pp. 15–113. doi: 10.1016/B978-0-12-546801-5.50008-6.

[31] R. A. Dickie, "Mechanical Properties (Small Deformations) of Multiphase Polymer Blends," in *Polymer Blends*, Elsevier, 1978, pp. 353–391. doi: 10.1016/B978-0-12-546801-5.50014-1.

[32] H. Tanaka, A. J. Lovinger, and D. D. Davis, "Miscibility and Isomorphic Cocrystallization in Blends of Ferroelectric Copolymers of Vinylidene Fluoride and Trifluoroethylene."

[33] L. M. P. Pinheiro, M. R. Chaud, R. Gregório Filho, and P. A. P. Nascente, "Miscibility and Morphology of PVDF/P(VDF-TrFE) Blends," *Materials Science Forum*, vol. 403, pp. 83–88, Jul. 2002, doi: 10.4028/www.scientific.net/MSF.403.83.

[34] X. Zhang, W. Dong, Y. Liu, G. Xu, and H. Xu, "Structural and ferroelectric behaviours in blends of vinylidene fluoride oligomer and poly(vinylidene fluoride-trifluoroethylene) copolymer thin film," *Journal of Physics D: Applied Physics*, vol. 44, no. 43, Nov. 2011, doi: 10.1088/0022-3727/44/43/435304.

[35] N. Jia, Q. He, J. Sun, G. Xia, and R. Song, "Crystallization behavior and electroactive properties of PVDF, P(VDF-TrFE) and their blend films," *Polymer Testing*, vol. 57, pp. 302–306, Feb. 2017, doi: 10.1016/j.polymertesting.2016.12.003.

[36] K. E. Park, M. G. Kim, and B. E. Park, "Characterizations of blended PVDF/P(VDF-TrFE) films for ferroelectric organic field-effect transistors," *Journal of Semiconductor Technology and Science*, vol. 19, no. 3, pp. 287–291, Jun. 2019, doi: 10.5573/JSTS.2019.19.3.287.

[37] F. Kibria, W. Rahman, and S. N. Patra, "Detection of high sensitive acoustic region for sensible applications of electrospinning based PVDF-TrFE nanofiber sensor," *Nano Express*, vol. 1, no. 2, p. 020027, Aug. 2020, doi: 10.1088/2632-959x/abad00.

[38] G. Suresh, G. Mallikarjunachari, S. Jatav, C. Thirmal, M. S. Ramachandra Rao, and D. K. Satapathy, "Evolution of morphology, ferroelectric, and mechanical properties in poly(vinylidene fluoride)–poly(vinylidene fluoride-trifluoroethylene) blends," *Journal of Applied Polymer Science*, vol. 135, no. 10, Mar. 2018, doi: 10.1002/app.45955.

[39] N. Soin *et al.*, "Exclusive self-aligned β-phase PVDF films with abnormal piezoelectric coefficient prepared via phase inversion," *Chemical Communications*, vol. 51, no. 39, pp. 8257–8260, May 2015, doi: 10.1039/c5cc01688f.

[40] S. Badatya, D. K. Bharti, A. K. Srivastava, and M. K. Gupta, "Solution processed high performance piezoelectric eggshell membrane – PVDF layer composite nanogenerator via tuning the interfacial polarization," *Journal of Alloys and Compounds*, vol. 863, May 2021, doi: 10.1016/j.jallcom.2020.158406.

[41] J. Huang *et al.*, "Optimization Model for Flexible Piezoelectric Film in Self-Powered Pressure Sensor."

[42] T. Nishiyama, T. Sumihara, E. Sato, and H. Horibe, "Effect of solvents on the crystal formation of poly (vinylidene fluoride) film prepared by a spin-coating process," *Polymer Journal*, vol. 49, no. 3, pp. 319–325, Mar. 2017, doi: 10.1038/pj.2016.116.

[43]   Z. Du, C. J. Janke, J. Li, C. Daniel, and D. L. W. Iii, "Electron beam curing of composite positive electrode for Li-ion battery." [Online]. Available: http://energy.gov/downloads/doe-public-access-plan

[44]   S. Lobe, A. Bauer, S. Uhlenbruck, and D. Fattakhova-Rohlfing, "Physical Vapor Deposition in Solid-State Battery Development: From Materials to Devices," *Advanced Science*, vol. 8, no. 11. John Wiley and Sons Inc, Jun. 01, 2021. doi: 10.1002/advs.202002044.

[45]   T. Boccaccio, A. Bottino, G. Capannelli, and P. Piaggio, "Characterization of PVDF membranes by vibrational spectroscopy," 2002.

[46]   A. Salimi and A. A. Yousefi, "FTIR studies of β-phase crystal formation in stretched PVDF films," *Polymer Testing*, vol. 22, no. 6, pp. 699–704, Sep. 2003, doi: 10.1016/S0142-9418(03)00003-5.

[47]   A. Srivastava, K. K. Jana, P. Maiti, D. Kumar, and O. Parkash, "Poly(vinylidene fluoride)/ CaCu3Ti4O12 and la doped CaCu3Ti4O12 composites with improved dielectric and mechanical properties," *Materials Research Bulletin*, vol. 70, pp. 735–742, Jun. 2015, doi: 10.1016/j.materresbull.2015.05.030.

[48]   X. Cai, T. Lei, D. Sun, and L. Lin, "A critical analysis of the α, β and γ phases in poly(vinylidene fluoride) using FTIR," *RSC Advances*, vol. 7, no. 25, pp. 15382–15389, 2017, doi: 10.1039/c7ra01267e.

[49]   D. Vatansever, R. L. Hadimani, T. Shah, and E. Siores, "Characterisation of energy generating PolyVinylidene Fluoride (PVDF) based piezoelectric filament," in *Advanced Materials Research*, 2012, vol. 410, pp. 366–369. doi: 10.4028/www.scientific.net/AMR.410.366.

[50]   C. K. McGinn *et al.*, "Formulation, printing, and poling method for piezoelectric films based on PVDF–TrFE," *Journal of Applied Physics*, vol. 128, no. 22, p. 225304, Dec. 2020, doi: 10.1063/5.0027855.

[51]   R. L. Hadimani *et al.*, "Continuous production of piezoelectric PVDF fibre for e-textile applications," *Smart Materials and Structures*, vol. 22, no. 7, Jul. 2013, doi: 10.1088/0964-1726/22/7/075017.

[52]   X. Hu, M. You, N. Yi, X. Zhang, and Y. Xiang, "Enhanced Piezoelectric Coefficient of PVDF-TrFE Films via In Situ Polarization," *Frontiers in Energy Research*, vol. 9, Aug. 2021, doi: 10.3389/fenrg.2021.621540.

[53]   I. Katsouras *et al.*, "The negative piezoelectric effect of the ferroelectric polymer poly(vinylidene fluoride)," *Nature Materials*, vol. 15, no. 1, pp. 78–84, Jan. 2016, doi: 10.1038/nmat4423.

[54]   I. Urbanaviciute *et al.*, "Negative piezoelectric effect in an organic supramolecular ferroelectric," *Materials Horizons*, vol. 6, no. 8, pp. 1688–1698, Oct. 2019, doi: 10.1039/c9mh00094a.

[55]   W. J. Hu *et al.*, "Universal ferroelectric switching dynamics of vinylidene fluoride-trifluoroethylene copolymer films," *Scientific Reports*, vol. 4, Apr. 2014, doi: 10.1038/srep04772.

[56]   H. Su, A. Strachan, and W. A. Goddard, "Density functional theory and molecular dynamics studies of the energetics and kinetics of electroactive polymers: PVDF and P(VDF-TrFE)," *Physical Review B - Condensed Matter and Materials Physics*, vol. 70, no. 6, Aug. 2004, doi: 10.1103/PhysRevB.70.064101.

[57]   Y. J. Yu and A. J. H. McGaughey, "Energy barriers for dipole moment flipping in PVDF-

related ferroelectric polymers," *Journal of Chemical Physics*, vol. 144, no. 1, Jan. 2016, doi: 10.1063/1.4939152.

[58] S. Lanceros-Méndez, J. F. Mano, A. M. Costa, and V. H. Schmidt, "FTIR and DSC studies of mechanically deformed β-PVDF films," *Journal of Macromolecular Science - Physics*, vol. 40 B, no. 3–4, pp. 517–527, May 2001, doi: 10.1081/MB-100106174.

[59] S. Barrau *et al.*, "Nanoscale Investigations of α- And γ-Crystal Phases in PVDF-Based Nanocomposites," *ACS Applied Materials and Interfaces*, vol. 10, no. 15, pp. 13092–13099, Apr. 2018, doi: 10.1021/acsami.8b02172.

[60] S. K. Mahadeva, J. Berring, K. Walus, and B. Stoeber, "Effect of poling time and grid voltage on phase transition and piezoelectricity of poly(vinyledene fluoride) thin films using corona poling," *Journal of Physics D: Applied Physics*, vol. 46, no. 28, Jul. 2013, doi: 10.1088/0022-3727/46/28/285305.

[61] B. Mahale, D. Bodas, and S. A. Gangal, "Study of β-phase development in spin-coated PVDF thick films," *Bulletin of Materials Science*, vol. 40, no. 3, pp. 569–575, Jun. 2017, doi: 10.1007/s12034-017-1390-4.

[62] L. Ruan, X. Yao, Y. Chang, L. Zhou, G. Qin, and X. Zhang, "Properties and applications of the β phase poly(vinylidene fluoride)," *Polymers*, vol. 10, no. 3. MDPI AG, Feb. 26, 2018. doi: 10.3390/polym10030228.

[63] B. Luo, X. Wang, Y. Wang, and L. Li, "Fabrication, characterization, properties and theoretical analysis of ceramic/PVDF composite flexible films with high dielectric constant and low dielectric loss," *Journal of Materials Chemistry A*, vol. 2, no. 2, pp. 510–519, Jan. 2014, doi: 10.1039/c3ta14107a.

[64] P. Nallasamy, "Vibrational spectroscopic characterization of form II poly(vinylidene fluoride)," 2005.

[65] D. Mao, B. E., and M. A., "Ferroelectric Properties and Polarization Switching Kinetic of Poly (vinylidene fluoride-trifluoroethylene) Copolymer," in *Ferroelectrics - Physical Effects*, InTech, 2011. doi: 10.5772/17147.
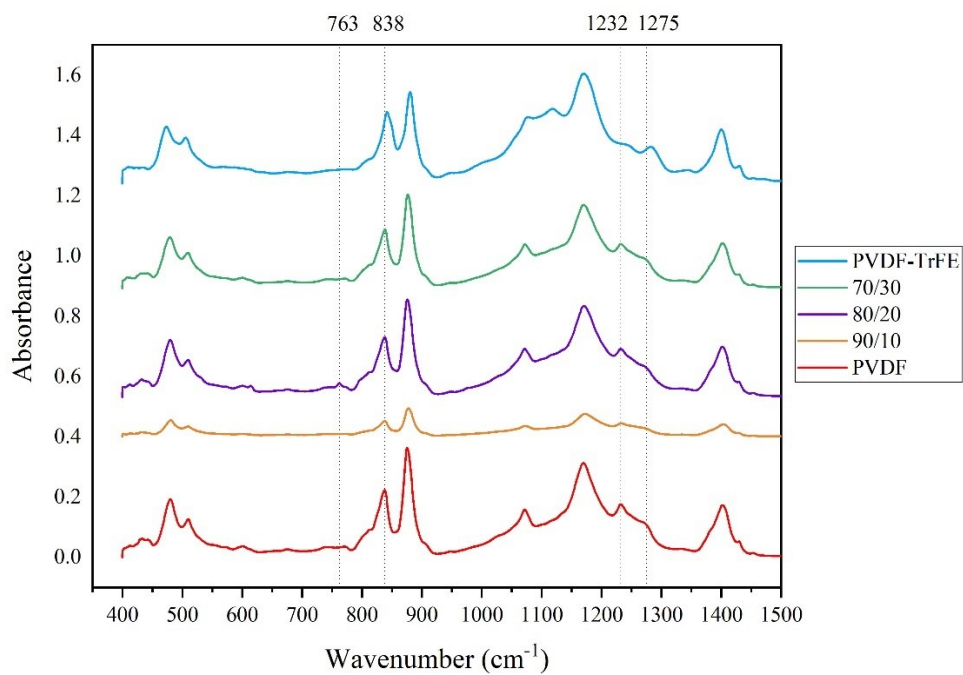
Appendix

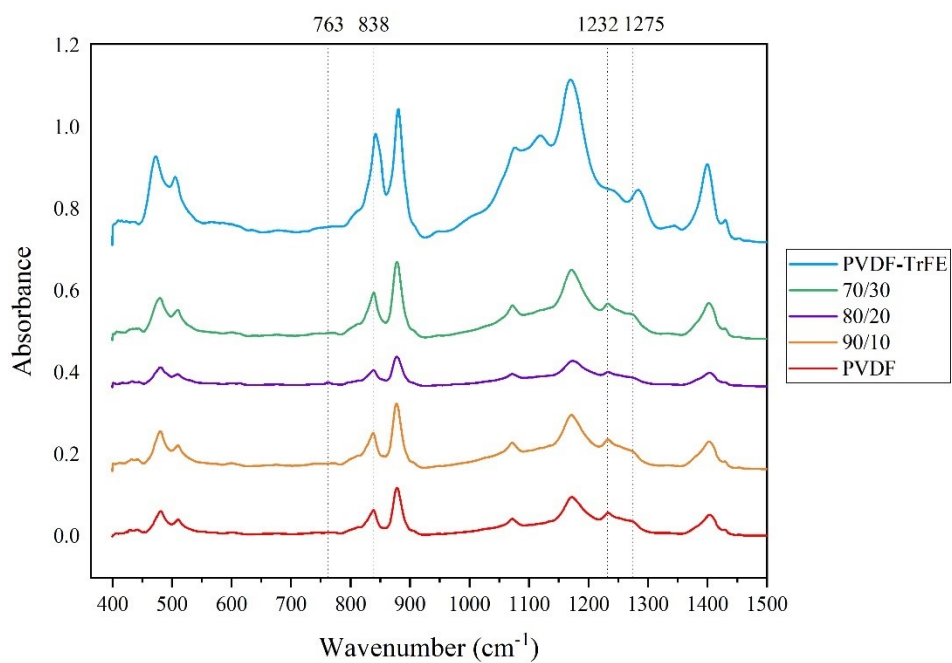Figure A1. The FT-IR graph of samples with different weight ratios under poling.

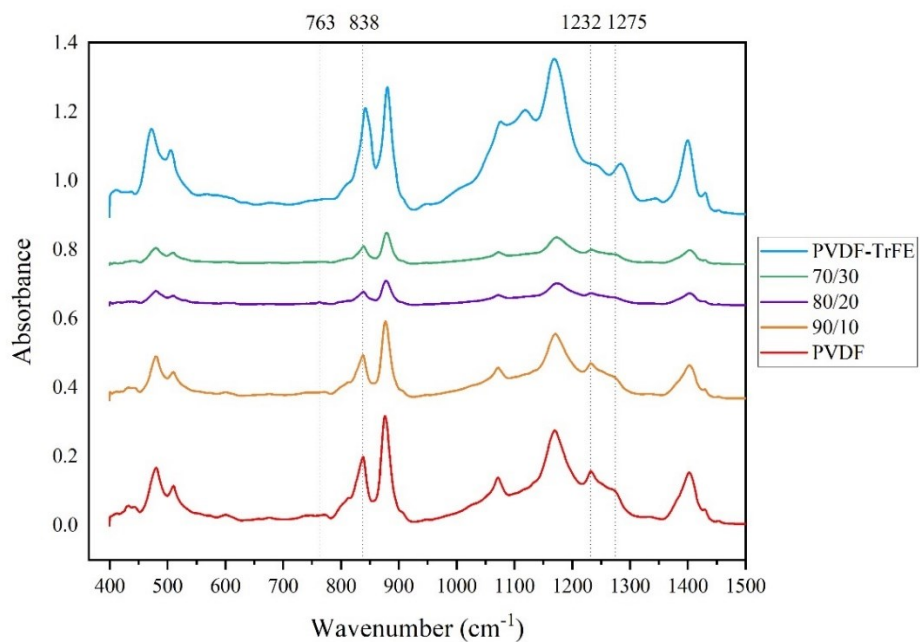Figure A2. The FT-IR graph of samples with different weight ratios under annealing poling.

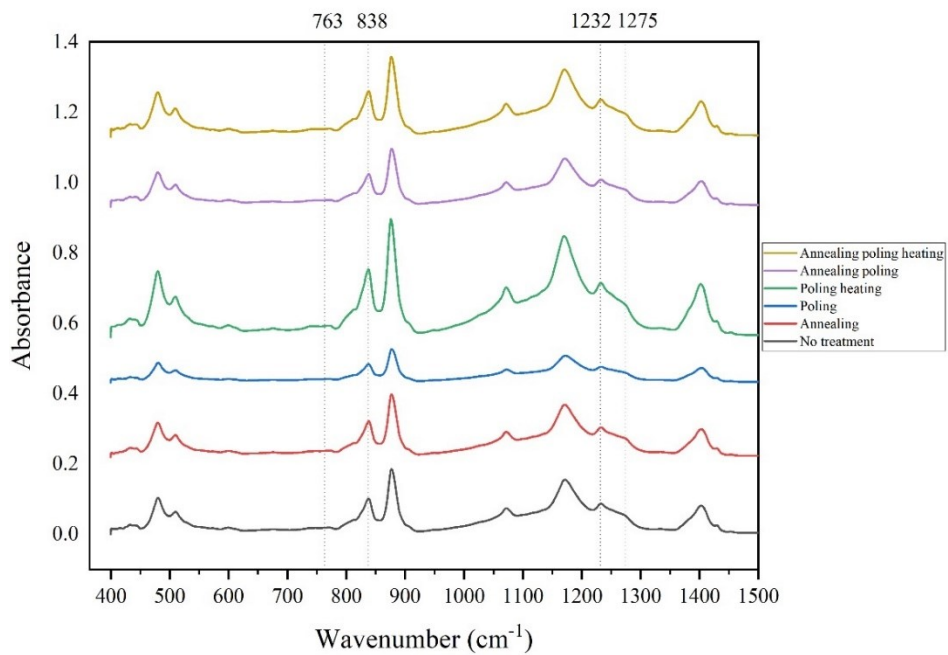Figure A3. The FT-IR graph of samples with different weight ratios under annealing poling heating.

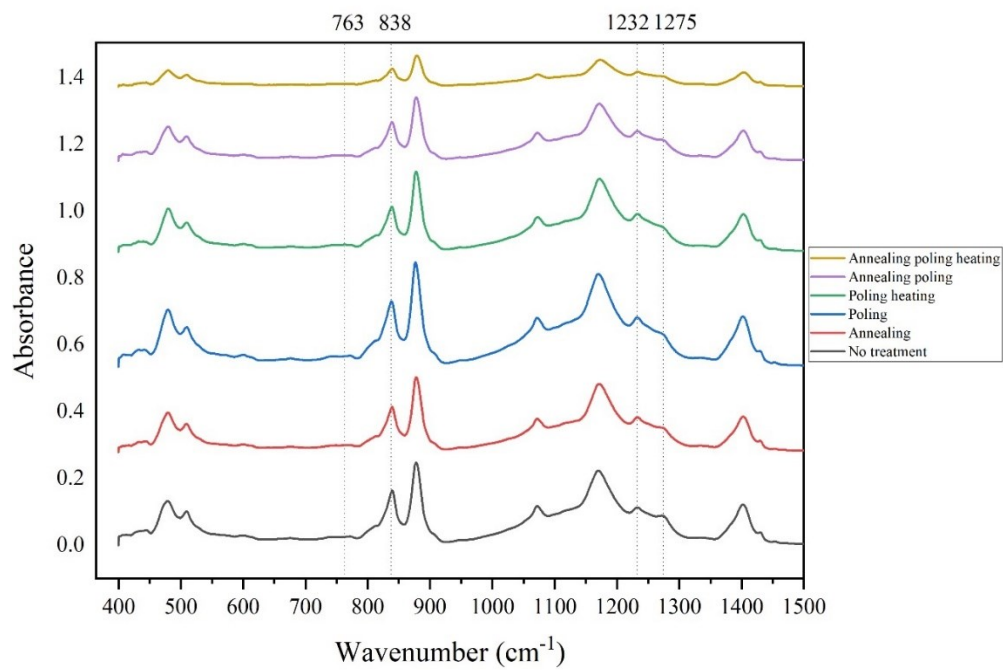Figure A4. The FT-IR graph of 90/10 samples under different treatments.

Figure A5. The FT-IR graph of 70/30 samples under different treatments.